REGULATION OF EXPRESSION AND REGULATED INTRAMEMBRANE PROTEOLYSIS OF CREB3L1

APPROVED BY SUPERVISORY COMMITTEE

Jin Ye, Ph.D.

Guosheng Liang, Ph.D.

Zhijian Chen, Ph.D.

Julie Pfeiffer, Ph.D.

Mamta Jain, M.D.

To my parents and sister, for their love and support.

REGULATION OF EXPRESSION AND REGULATED INTRAMEMBRANE PROTEOLYSIS OF CREB3L1

by

QIUYUE CHEN

DISSERTATION

Presented to the Faculty of the Graduate School of Biomedical Sciences

The University of Texas Southwestern Medical Center at Dallas

In Partial Fulfillment of the Requirements

For the Degree of

DOCTOR OF PHILOSOPHY

The University of Texas Southwestern Medical Center

Dallas, Texas

August, 2013

ACKNOWLEDGEMENT

My sincere gratitude goes to my supervisor Dr. Jin Ye, whose guidance and wisdom helped me to finish these projects. I have learned a lot from him throughout the years in his lab. His passion about science has encouraged me to keep pushing the boundaries of my work. If it were not for his critical thinking and broad knowledge, this dissertation would not have been possible. I am extremely grateful for his patience and support during the past few years.

I would also like to thank my dissertation committee members Dr. Guosheng Liang, Dr. Zhijian Chen, Dr. Julie Pfeiffer, and Dr. Mamta Jain, for their time and invaluable advice.

I thank all the members in the Ye lab, past and present, especially Dr. Joon No Lee, Dr. Bray Denard, Dr. Hyeonwoo Kim, Saada Abdalla and Ellen Lee, for their advice, assistance, encouragement and friendship. They made the lab a fun place to learn and experience science.

REGULATION OF EXPRESSION AND REGULATED INTRAMEMBRANE PROTEOLYSIS OF CREB3L1

QIUYUE CHEN, Ph.D.

The University of Texas Southwestern Medical Center at Dallas, 2013

JIN YE, Ph.D.

cAMP response element binding protein 3-like 1 (CREB3L1) is a transcription factor synthesized as a membrane-bound precursor and activated through Regulated Intramembrane Proteolysis (RIP). Previous study has shown that CREB3L1 was proteolytically cleaved upon viral infection, allowing its NH_2-terminus to enter nucleus to drive genes encoding inhibitors of the cell cycles. As a result, CREB3L1 inhibited replication of cells infected by some virus including Hepatitis C virus (HCV). HCV does not replicate efficiently in wild-type human hepatoma Huh-7 cells, but it replicates robustly in certain subclones of Huh-7 cells. It is found that the expression of CREB3L1 is blocked in the cells permissive for HCV replication. However, how CREB3L1 is silenced in those cells remains unknown. Here we showed that CREB3L1 and other anti-viral genes like myxovirus resistant 1 (MX1) were epigenetically silenced through DNA methylation in different subclones that are permissive for HCV replication. Methylation microarray analysis suggested that Huh-7 cells existed as a mixed population of cells with

distinct patterns of gene methylation. This result indicates that subclones of Huh-7 cells become highly permissive for HCV replication by having their antiviral genes epigenetically silenced through DNA hypermethylation.

In addition to driving transcription of genes encoding inhibitors of cell cycle, activation of CREB3L1 also induces the expression of genes involved in assembly of collagen matrix. Transforming growth factor-β (TGF-β) is well known to induce excessive synthesis of collagen causing tissue fibrosis. We found that sustained induction of collagen synthesis by TGF-β required proteolytic activation of CREB3L1. RIP of CREB3L1 was inhibited by transmembrane 4 L6 family member 20 (TM4SF20), which retained CREB3L1 in the endoplasmic reticulum thereby separating CREB3L1 from the Golgi-resident proteases catalyzing the RIP reaction. TGF-β inhibited TM4SF20 expression through activation of extracellular signal-regulated kinases to stimulate RIP of CREB3L1. This cleavage allowed the NH_2-terminal fragment of CREB3L1 to enter the nucleus where it forms a complex with Smad4 to activate transcription of genes involved in assembly of collagen extracellular matrix. Our study suggests that RIP of CREB3L1 could be a drug target to treat tissue fibrosis.

Doxorubicin, a drug used in chemotherapy, is found to inhibit cell proliferation by inducing synthesis of ceramide, which in turn activates RIP of CREB3L1. Yet the mechanism through which ceramide activates CREB3L1 is not clear. Here we reported that ceramide induced alternative translocation of TM4SF20: In the absence of ceramide, the NH_2-terminus of TM4SF20 was used as signal sequence to insert the polytopic membrane protein into ER. Upon treatment of ceramide, the NH_2-terminus of TM4SF20 was no longer recognized as signal sequence. Instead, the NH_2-terminus of newly synthesized TM4SF20 proteins was located in the cytosol, resulting in alternative translocation of the protein that adopted a membrane topology opposite to that in the absence of the lipid. We further demonstrated that insertion of the NH_2-terminal sequence of TM4SF20 into ER in the absence of ceramide required translocation associated membrane protein 2 (TRAM2), as knockdown of TRAM2 led

to alternative translocation of TM4SF20 even in the absence of ceramide. Since TRAM2 contains a domain known to bind ceramide, we suspect that ceramide may inhibit the function of TRAM2. These results suggest that ceramide could induce RIP of CREB3L1 by inactivating TM4SF20 through alternative translocation.

TABLE OF CONTENTS

PRIOR PUBLICATIONS

Chen, Q., Denard, B., Huang, H., and Ye, J. (2013). Epigenetic silencing of antiviral genes renders clones of Huh-7 cells permissive for hepatitis C virus replication. J Virol *87*, 659-665.

Denard, B., Seemann, J., **Chen, Q.**, Gay, A., Huang, H., Chen, Y., and Ye, J. (2011). The membrane-bound transcription factor CREB3L1 is activated in response to virus infection to inhibit proliferation of virus-infected cells. Cell Host Microbe *10*, 65-74.

Cui, J., **Chen, Q.**, Yue, X., Jiang, X., Gao, G.F., Yu, L.C., and Zhang, Y. (2010). Galanin protects against intracellular amyloid toxicity in human primary neurons. J Alzheimers Dis *19*, 529-544.

Cui, J., **Chen, Q.**, Yu, L.C., and Zhang, Y. (2008). Chronic morphine application is protective against cell death in primary human neurons. Neuroreport *19*, 1745-1749.

Chen, Q., Cui, J., Zhang, Y., and Yu, L.C. (2008). Prolonged morphine application modulates Bax and Hsp70 levels in primary rat neurons. Neurosci Lett *441*, 311-314.

Zhang, Y., **Chen, Q.**, and Yu, L.C. (2008). Morphine: a protective or destructive role in neurons? Neuroscientist *14*, 561-570.

LIST OF FIGURES

APPENDICES

LIST OF ABBREVIATIONS

ADAM19, ADAM metallopeptidase domain 19
BMP 2, bone morphogenetic protein 2
CHRNA9, cholinergic receptor nicotinic α9
CLDN4, claudin 4
COL1A1, collagen 1α1
CREB3L1, cAMP response element binding protein 3-like 1
ECM, extracellular matrix
EMCV, encephalomyocarditis virus
EMT, epithelial-mesenchymal transition
ER, endoplasmic reticulum
ERKs, extracellular signal-regulated kinases
HCC, hepatocellular carcinoma
HCV, Hepatitis C virus
IFN, Interferon
IRES, Internal Ribosome Entry Site
ISGs, Interferon-Stimulated-Genes
LRRC8C, leucine rich repeat containing 8 family member C
MX1, myxovirus resistant 1
OAS, 2', 5'-oligoadenylate-synthetase
PKR, protein kinase R
RdRp, RNA-dependent RNA polymerase
RIP, Regulated Intramembrane Proteolysis
S1P, site-1 protease
S2P, site-2 protease
SMase, sphingomyelinase
SPARC, Secreted protein, acidic, cysteine-rich
SPT, serine palmitoyl transferase
SR, SRP receptor
SREBPs, sterol regulatory element binding proteins
SRP, signal recognition particle
SVR, sustained virological response
TGF-β, Transforming growth factor-β
TLC, TRAM-Lag1p-CLN8
TM4SF20, transmembrane 4 L6 family member 20
TRAM2, translocation associated membrane protein 2
UTR, untranslated region

CHAPTER ONE:

Introduction

1.1 Regulated Intramembrane Proteolysis

Regulated intramembrane proteolysis (RIP) is a signaling pathway through which cells transmit signals from the endoplasmic reticulum (ER) to nucleus. The first and best characterized RIP dependent signaling pathway is the proteolytic activation of the sterol regulatory element binding proteins (SREBPs). SREBPs are transmembrane proteins locating in the ER. When cells are loaded with sterols, SREBPs reside in the ER. When cells are depleted with sterols, SREBPs translocate from the ER to Golgi, where they are sequentially cleaved by site-1 protease (S1P) and site-2 protease (S2P). This results in release of the NH_2-terminal fragment of SREBPs from membranes, allowing it to enter the nucleus to activate transcription of genes involved in sterol synthesis (Ye and DeBose-Boyd, 2011). CREB3L1 is also a membrane-bound transcription factor that is activated by RIP. It has been shown that CREB3L1 undergoes RIP in response to viral infection to inhibit proliferation of virus-infected cells (Denard et al., 2011). Proteolytic activation of CREB3L1 is also responsible for doxorubicin, a drug wildly used for cancer treatment, to prevent growth of cancer cells. Doxorubicin induces RIP of CREB3L1 by stimulating synthesis of ceramide (Denard et al., 2012).

RIP is a highly regulated process. Not surprisingly, a lot of regulatory proteins are involved in this process. Well-characterized RIP of SREBPs is controlled by two transmembrane proteins: Scap and Insig. Scap forms a complex with SREBP. In cells repleted with sterols, Insig binds to Scap in the ER, preventing translocation of Scap/SREBP from ER to Golgi. In sterol-depleted cells, Scap/SREBP dissociates from Insig, allowing the complex to be transported to Golgi where SREBP undergoes

proteolytic cleavage (Ye and DeBose-Boyd, 2011). Despite the discovery of Scap and Insig, regulatory proteins involved in RIP of CREB3L1 remain unknown.

1.2 Hepatitis C virus and antiviral genes

Hepatitis C Virus (HCV) infects about 170 million people worldwide and it is a major cause of chronic liver fibrosis, cirrhosis and hepatocellular carcinoma (HCC) (Chen and Morgan, 2006). HCV is a positive, single stranded RNA virus. Its 9.6 kb-genome is composed of a 5'UTR including an Internal Ribosome Entry Site (IRES), an open reading frame that encodes structural and non-structural proteins, and a 3' UTR. IRES initiates the translation of a single polyprotein which is processed into structural proteins and non-structural proteins. (Lindenbach and Rice, 2005; Moradpour et al., 2007). HCV are classified into different genotypes and subtypes based on their nucleotide sequence. There are six major genotypes and are further characterized into subtypes (Moradpour et al., 2007).

Host cells recognize the invasion of viruses and mount antiviral responses. The innate immune system is essential for detection of viruses and initiation of expression of antiviral genes. Interferons (IFNs) are important cytokines that are recognized as key components in innate immunity. Three classes of IFN have been identified, namely type I to III. Four main effector-pathways of the IFN-mediated antiviral pathways are identified: the Mx GTPase pathway, the 2', 5'-oligoadenylate-synthetase (OAS) directed ribonuclease L pathway, the protein kinase R (PKR) pathway, and the Interferon-Stimulated-Genes (ISGs) pathway (Katze et al., 2002; Sadler and Williams, 2008). One of the type I interferon, IFN-α, in combination with ribavirin have been used for a long time as a therapy for HCV infection. However, this therapy is associated with significant adverse effects and leads to sustained virological response (SVR) in only 50% of patients with infection of genotype 1 HCV (Lauer and Walker, 2001). Failure of this treatment in some patients requests more efficient drugs. Due to the high mutation rate of HCV genome, drugs targeting viral proteins may lead to drug resistance. Therefore, studying host factors would

reveal more insights in drug development because drugs targeting host factors may not be affected by mutations in viral genome.

Human hepatoma Huh-7 cells are used to study HCV replication *in vitro*. HCV does not replicate efficiently in wild-type Huh-7 cells, but it replicates robustly in certain subclones of Huh-7 cells. Comparison between parental Huh-7 cells and permissive subclones of the cells has been used to identify important host factors required for HCV replication. One permissive line, namely Huh-7.5, was found to be defective in producing type I interferon in response to viral infection as a result of a dominant negative mutation of an antiviral genes, *RIG-I* (Sumpter et al., 2005). Later, comparisons between HPR1, another permissive cell line, and Huh-7 led to identification of an antiviral gene named CREB3L1 (Denard et al., 2011). Viral infection induces RIP of CREB3L1, and the NH_2-terminus of CREB3L1 enters the nucleus to activate genes encoding cell-cycle inhibitors to prevent proliferation of virus-infected cells. However, how expressions of these antiviral genes are inhibited in permissive cell lines is unknown.

1.3 TGF-beta signaling and fibrosis

Transforming growth factor-β (TGF-β) is a secreted polypeptide that activates cellular responses during growth and differentiation. Mature TGF-β is a homodimer of two 12.5-kd polypeptides joined by a disulfide bond. TGF-β proteins signal through cell surface complexes of two types of receptors, namely type I and type II receptors, respectively. Type I and type II receptors exist as homodimers at the cell surface without ligands. TGF-β binds efficiently to type II receptors and stabilizes the type II-type I receptor heterodimer (Feng and Derynck, 2005). Upon ligand binding, type II receptors phosphorylate serine and threonine residues of type I receptors, and the activated receptors signal through the canonical Smad pathway to regulate gene expression. Specifically, activated type I receptors recruit and phosphorylate R-Smad, Smad2 and Smad3. Upon releasing from the receptors, the phosphorylated R-Smad forms a complex with a co-Smad, Smad4. This heterodimer enters nucleus to induce gene expression (Feng and Derynck, 2005; Massague, 2012).

Except for the canonical Smad pathways, TGF-β also signals through a non-canonical pathway in which TGF-β activates extracellular signal-regulated kinases (ERKs) (Derynck and Zhang, 2003; Mu et al., 2012). In addition to the phosphorylation of serine/threonines of type I receptors, type II receptors are autophosphorylated on three tyrosine residues upon activation, which results in the recruitment of several adaptor proteins that have been implicated in the activation of Erk-MAPK signaling pathways (Mu et al., 2012).

Fibrosis is a pathological scaring process, during which excessive extracellular matrix (ECM) is deposited and leads to organ failure (Zeisberg and Kalluri, 2013). Fibrosis plays an important role in the progression of many chronic diseases in parenchymal organs such as liver, lung, kidney, and heart (Zeisberg and Kalluri, 2013). In fibrosis, the principal source of collagen, a major component of ECM, is activated fibroblasts (Kisseleva and Brenner, 2008; Zeisberg and Kalluri, 2013). Activated fibroblasts may originate from resident fibroblasts, bone marrow-derived fibrocytes, and epithelial cells (Kisseleva and Brenner, 2008). Epithelial cells contribute to fibroblast accumulation through epithelial-mesenchymal transition (EMT) (Kisseleva and Brenner, 2008), a process known to be activated by TGF-β (Bi et al., 2012; Chapman, 2011). TGF-β has been found to play a prominent role in inducing collagen synthesis in fibrogenesis (Araya and Nishimura, 2010; Dooley and ten Dijke, 2012; Edgley et al., 2012; Lan, 2011).

1.4 Possible role of CREB3L1 in fibrosis

Type I collagen, Col1a1, is known to be a target gene of CREB3L1 (Denard et al., 2011; Murakami et al., 2009). CREB3L1 knockout mice exhibited severe osteopenia, caused by a decrease of type I collagen in the bone matrix (Murakami et al., 2009). Secreted protein, acidic, cysteine-rich (SPARC), a protein directly affecting procollagen processing and therefore assembly of collagen extracelluar matrix (Rentz et al., 2007), is also identified as a target of CREB3L1 (Denard et al., 2011). Although the role of CREB3L1 in bone development is characterized, how CREB3L1 affects TGF-β-mediated fibrotic development has never been examined.

1.5 Role of ceramide in activating RIP of CREB3L1

Ceramide is a sphingolipid consisting of sphingosine, an 18-carbon unsaturated amino alcohol hydrocarbon chain, joined by an amide linkage to a fatty acid of varying chain length and a varying degree of saturation (Morad and Cabot, 2013). It can be generated by the breakdown of sphingomyelin by sphingomyelinase (SMases) on the plasma membrane. Ceramide is also synthesized *de novo* by serine palmitoyl transferase (SPT) and ceramide synthases (Hannun and Obeid, 2008). *De novo* synthesis happens in the ER (Hannun and Obeid, 2008). Ceramide is known to have signaling activity. For example, ceramide has been shown to inhibit cell proliferation (Morad and Cabot, 2013). In general, lipids affect biological functions through two mechanisms: first, lipid-lipid interaction results in structural change of membrane therefore affect functions of transmembrane proteins. Second, lipid-protein interaction directly affects target proteins. It has been found that doxorubicin, a drug wildly used for chemotherapy, increased *de novo* synthesis of ceramide, which in turn robustly induced RIP of CREB3L1 (Denard et al., 2012). However, the underlying mechanism remains unclear.

CHAPTER TWO:

Antiviral Genes Are Epigenetically Silenced in HCV Permissive Cells

2.1 Abstract

Hepatitis C virus (HCV) does not replicate efficiently in wild-type human hepatoma Huh-7 cells, but it replicates robustly in certain subclones of Huh-7 cells. Previously, we demonstrated that silencing of cyclic AMP (cAMP) response element binding protein 3-like 1 (*CREB3L1*), a cellular transcription factor that inhibits HCV replication, allows HCV to replicate in HRP1 cells, a subclone of Huh-7 cells permissive for HCV replication. Here we show that silencing of myxovirus resistant 1 (*MX1*), a known interferon-induced antiviral gene, is responsible for HRP4 cells, another subclone of Huh-7 cells, being permissive for HCV replication. Both *CREB3L1* and *MX1* are epigenetically silenced through DNA methylation in HRP1 and HRP4 cells, respectively. We further demonstrate that Huh-7 cells exist as a mixed population of cells with distinct patterns of gene methylation and HCV replicates in subpopulations of Huh-7 cells that have antiviral genes epigenetically silenced by DNA hypermethylation. Our results demonstrate that understanding the mechanism through which subclones of Huh-7 cells become permissive for HCV replication is crucial for studying their interaction with HCV.

2.2 Introduction

A powerful approach to study innate antiviral response is to compare wild-type Huh-7 cells, which do not support robust replication of hepatitis C virus (HCV), and certain subclones of Huh-7 cells that are permissive for HCV replication. The subclones of Huh-7 cells that support HCV replication can be selected by an HCV subgenomic replicon that consists of HCV RNA engineered to express a selectable marker gene, *neo*, in place of a portion of the viral RNA that is not required for viral replication(Lohmann et al., 1999). When Huh-7 cells were transfected with the HCV replicon RNA, followed by G418 selection, only a few cells survived the selection, an observation suggesting that most Huh-7 cells are not permissive for HCV replication(Blight et al., 2002; Lohmann et al., 1999). When HCV RNA was eliminated from the surviving cells through interferon treatment, the cured cells showed dramatically enhanced permissiveness for HCV RNA replication, as demonstrated by the large number of cells that survived G418 selection following retransfection with the HCV replicon RNA(Blight et al., 2002). Huh-7.5 cells are a line of these cured cells(Blight et al., 2002). Unlike parental Huh-7 cells, Huh-7.5 cells failed to produce type 1 interferon in response to viral infection as a result of a dominant negative mutation in the *RIG-I* gene(Sumpter et al., 2005).

However, the mutation in *RIG-I* alone is not sufficient to make Huh-7 cells permissive for HCV replication(Binder et al., 2007; Denard et al., 2011). We recently observed that cyclic AMP (cAMP) response element binding protein 3-like 1 (CREB3L1) is expressed in parental Huh-7 cells but not in Huh-7.5 cells and another subclone of Huh-7 cells supporting HCV replication, namely, HRP1 cells(Denard et al., 2011). CREB3L1 is synthesized as a membrane-bound precursor. It is proteolytically activated in virus-infected cells so that the NH_2-terminal domain of the protein is able to enter the nucleus to activate transcription of genes encoding proteins that block the cell cycle (Denard et al., 2011). Inasmuch as active division of host cells is required for efficient HCV replication (Pietschmann et al., 2001; Scholle et al., 2004), activation of CREB3L1 not only blocks proliferation of HCV-infected cells

but also inhibits viral replication (Denard et al., 2011). As a result, expression of *CREB3L1* must be silenced in cells highly permissive for HCV replication so that they are able to divide while supporting efficient viral replication. However, how expression of*CREB3L1* is silenced in these cells remains a mystery.

Cytosine methylation is a major epigenetic mechanism to regulate gene expression (Deaton and Bird, 2011). In mammalian cells, cytosine methylation occurs at CpG dinucleotides, which are concentrated in small CpG-rich regions. These regions, which are designated CpG islands, are often associated with gene promoters. Methylation of the cytosines in CpG islands results in transcriptional repression of the gene (Deaton and Bird, 2011).

In the current study, we determine that *CREB3L1* in HRP1 cells is silenced through gene methylation. Hypermethylation of myxovirus resistant 1 (*MX1*), an interferon-induced antiviral gene, also allows HCV to replicate in HRP4 cells, another subclone of Huh-7 cells permissive for HCV replication. We further demonstrate that Huh-7 cells are epigenetically unstable in that they exist as a heterogeneous population of cells with distinct patterns of DNA methylation. This instability may allow HCV to replicate in subpopulations of Huh-7 cells in which antiviral genes are epigenetically silenced by DNA hypermethylation.

2.3 Materials and Methods

Materials

We obtained 5-azacytide (5-azaC) and alpha interferon (IFN-α) from sigma and PBL Interferon Source, respectively.

Cell Culture

Huh-7, Huh-7.5, and HRP1 cells were maintained in medium A (Dulbecco' modified Eagle's medium with 4.5g/liter glucose, 100U/ml penicillin, 100µg/ml streptomycin sulfate, and 10% fetal calf serum). HRP4 HCV cells are a clone of Huh-7 cells transfected with the con1 HCV subgenomic replicon, followed by selection with 700µg/ml G418. HRP4 cells were generated after HRP4 HCV cells were treated with IFN-α for 2 weeks to remove the HCV replicon inside the cells. They were maintained in medium A. Huh-GL cells, a line of Huh-7 cells that contain a chromosomally integrated JFH-1 strain of HCV cDNA and constitutively produce infectious virus(Cai et al., 2005), were maintained in medium A supplemented with 5µg/ml blasticidin. HRP4/pMX1 and HRP4/pControl cells were generated by transfecting HRP4 cells with pCMV-MX1 (a plasmid encoding human MX1 driven by the cytomegalovirus promoter) and a control empty plasmid, respectively, followed by selection in medum A supplemented with 500µg/ml hygromycin. Huh-7/shControl and Huh-7/shMX1 cells were generated by transfecting Huh-7 cells with a control short hairpin RNA (shRNA) that does not target any human genes (SA biosciences) and an shRNA targeting MX1 (SA Biosciences, Clone ID 4), respectively, followed by selection in medium A supplemented with 500 µg/ml hygromycin. Huh-7/shMX1/pMX1 cells were generated by transfecting Huh-7/shMX1 cells with pCMV-MX1, followed by selection in medium A supplemented with 700 µg/ml of Zeocin. Huh-7/pNeo1 and Huh-7/pNeo2 cells were generated by transfecting Huh-7 cells with pcDNA3.1-neomycin, followed by selection in medium A supplemented with 500 µg/ml G418. All cells were cultured in monolayers at 37˚C in 5% CO_2.

Virus infection

The JFH-1 strain of HCV was produced from Huh7-GL cells as previously described (Huang et al., 2007). The HCV HP replicon RNA was *in vitro* transcribed as previously described (Sumpter et al., 2004) and transfected into Huh-7-derived cells suing TransMessenger reagent (Qiagen). Sendai virus (Cantell strain) was purchased from Charles River Laboratories. The virus was added to cells after it was diluted 50-fold in cell culture medium (3ml/60-mm plate).

Immunoblot analysis

Cell lysates were analyzed by 10% SDS-PAGE followed by immunoblot analysis with the indicated antibodies (1:2,000 dilution for anti-CREB3L (Denard et al., 2011) and 1: 10,000 dilution for anti-actin). Bound antibodies were visualized with a peroxidase-conjugated secondary antibody suing the SuperSignal enhanced chemiluminescence (ECL)-horseradish peroxidase (HRP) substrate system (Pierce).

Real-time qPCR

Real-time quantitative PCR (RT-qPCR) was performed as previously described (Liang et al., 2002). The relative amounts of RNAs were calculated through the comparative cycle threshold method by suing human 36B4 mRNA as the invariant control.

Luciferase assays

Luciferase activity in the cell lysate was assayed with the dual-luciferase reporter assay system (Promega) suing the synergy 4 plate reader and Gen5 1.10 software (BioTek). Promoter activity was determined by firefly luciferase activity normalized against *Renilla* luciferase activity to control for transfection efficiency.

G418 transduction efficiency assays

Quantification of the percentage of cells that survived G418 selection following transfection with a HCV replicon was performed exactly as previously described(Blight et al., 2002).

Microarray analysis

Microarray analysis was performed exactly as previously described (Horton et al., 2003).

Bisulfite sequencing

Genomic DNA was purified using the DNeasy blood and tissue kit (Qiagen) according to the manufacturer's protocol. DNA was then subject to bisulfite C→U conversion using the EZ DNA Methylation Gold kit (Zymo) according to the manufacturer's protocol. Treated and untreated DNA was used for PCR using ZymoTaq Premix (Zymo). Amplified fragments were ligated into a plasmid using the TOPO TA cloning kit (Invitrogen) for sequencing analysis.

DNA methylation microarray

Genomic DNA was purified using the DNeasy blood and tissue kit (Qiagen) according to the manufacturer's protocol. Genomic DNA (30 μg) was sonicated three times at 15% amplitude to break it into 300 bp to 1,000 bp (Brandson). The MeDIP kit (Diagenode) was used to immunoprecipitate methylated DNA. Both immunoprecipitated (IP) and input DNA was amplified with the WGA2 kit (Sigma). Amplified products were purified through the QIAquick PCR purification kit (Qiagen) and subjected to human DNA methylation 2.1 M deluxe promoter arrays analysis, performed by Roche NimbleGen. The signal intensity of methylation of a specific segment of DNA was determined by its $\log_2$ IP/input ratio.

Microarray data accession numbers

Microarray analyses comparing gene expression between Huh-7 and HRP4 cells treated with interferon or untreated were deposited at Gene Expression Omnibus (GEO) under accession number 31903. DNA methylation microarray analyses comparing gene methylation profiles among various subclones of Huh-7 cells were deposited at GEO under accession number 31960.

2.4 Results

CREB3L1 is hypermethylated in HRP1 cells.

To determine how expression of *CREB3L1* is suppressed in HRP1 cells, we performed extensive sequencing analysis but were unable to identify any mutation in the coding region or in the 5′ regulatory element of the gene in HRP1 cells. We thus considered the possibility that the gene was silenced through an epigenetic mechanism in these cells. Methylation of cytosines in CpG islands is a well-characterized epigenetic mechanism to suppress transcription of cellular genes (Deaton and Bird, 2011). *CREB3L1* contains a CpG island in its 5′ untranslated region (UTR) located in the first exon (Figure 1A). Bisulfite sequencing revealed that two cytosines in this region were methylated in more than 50% of the PCR clones amplified from the genomic DNA obtained from HRP1 cells (Figure 1A). Neither cytosine was methylated in the parental Huh-7 cells (Figure 1A). To confirm that hypermethylation of *CREB3L1* leads to inhibition of its expression, we treated the cells with 5-azaC, an inhibitor of DNA methylation (Christman, 2002). While having little impact on *CREB3L1* expression in Huh-7 cells, 5-azaC completely restored CREB3L1 expression in HRP1 cells by increasing its mRNA by ~100-fold (Figure 1B). The result shown in Figure 1 suggests that *CREB3L1* is epigenetically silenced in HRP1 cells through DNA methylation.

HRP4 cells are permissive for HCV replication.

To determine whether hypermethylation of an antiviral gene is unique in HRP1 cells or a common mechanism to generate subclones of Huh-7 cells permissive for HCV replication, we needed another line of Huh-7 cells also permissive for HCV replication but different from HRP1 cells. For this purpose, we transfected Huh-7 cells with an HCV subgenomic replicon RNA to obtain a line of Huh-7 cells that harbor the HCV replicon. These cells were treated with interferon to generate a clone of cured Huh-7 cells that no longer contained HCV RNA. These cells were designated HRP4 cells. HCV replicon RNA was

then retransfected into these cells to determine their permissiveness for HCV replication. Judged by the number of colonies that contained the HCV replicon carrying the *neo* gene, HRP4 cells were more permissive for HCV replication than their parental Huh-7 cells (Figure 2A and B). Quantification of the percentage of the cells that survived G418 selection indicated that HRP4 cells were as permissive as Huh-7.5 cells for replication of the HCV replicon (Figure 2B). HRP4 cells were also susceptible for infection by the JFH-1 strain of HCV, although the cells were not as supportive as Huh-7.5 cells for infection by this strain of HCV (Figure 2C). The observation that HRP4 cells are susceptible to infection by the JFH-1 strain of HCV suggests that they are different from HRP1 cells, because HRP1 cells are resistant to infection by the JFH-1 strain of HCV even though they are as permissive as Huh-7.5 cells for replication of the HCV subgenomic replicon (Denard et al., 2011). There is also a difference in CREB3L1 expression between the two lines of cells permissive for HCV replication: while the CREB3L1 protein was barely detectable by immunoblot analysis in both HRP1 and HRP4 cells (Figure 2D), the amount of CREB3L1 mRNA in HRP4 cells was much higher than that in HRP1 cells (Figure 2E).

HRP4 cells are defective in inducing MX1 expression in response to interferon.

We then analyzed the interferon response in HRP4 cells. For this purpose, we analyzed expression of *ISG56* and *MX1*, two well-characterized interferon-induced antiviral genes (Fensterl and Sen, 2011; Haller et al., 2007). Infection with Sendai virus, which stimulates production of interferon (Sumpter et al., 2005), activated expression of both *ISG56* and *MX1* in Huh-7 cells (Figure 3A). Sendai virus failed to induce these genes in Huh-7.5 cells (Figure 3A) because of a mutation in *RIG-I* that makes these cells defective in producing interferon in response to viral infection. Unlike Huh-7 or Huh-7.5 cells, Sendai virus stimulated expression only of *ISG56* and not of *MX1* in HRP4 cells (Figure 3A).

We then examined the effect of direct addition of IFN-α on expression of these genes. While IFN-α was equally potent in activating expression of *ISG56*in both Huh-7 and HRP4 cells (Figure 3B), it was much less effective in stimulating expression of *MX1* in HRP4 cells (Figure 3C). To determine whether

HRP4 cells are defective in activating expression of genes other than *MX1* in response to IFN-α, we performed microarray analysis to compare the effects of IFN-α on gene expression in Huh-7 and HRP4 cells. This analysis revealed that there were only two genes activated by interferon by more than 5-fold in Huh-7 cells that were not activated to the same degree in HRP4 cells (Table 1). Remarkably, *MX1* was one of the two genes. The other gene, *C1orf53*, has never been characterized.

Restoration of MX1 expression reduces the permissiveness of HRP4 cells for HCV replication.

To investigate whether the lack of *MX1* expression accounts for the permissiveness of HRP4 cells for HCV replication, we first determined whether restoration of *MX1* expression in these cells inhibited HCV replication. For this purpose, we stably transfected HRP4 cells with a plasmid encoding *MX1* and selected a clone of the cells expressing MX1 mRNA at a level similar to that in Huh-7 cells treated with interferon (Figure 4A). These cells, which were designated HRP4/pMX1, were transfected with an HCV subgenomic replicon RNA. Compared to HRP4 cells transfected with a control plasmid (HRP4/pControl), HRP4/pMX1 cells were much less permissive for HCV replication, as measured by the number of colonies that contained the HCV replicon (Figure 4B and C). These cells were also much more resistant to infection by the JFH-1 strain of HCV than HRP4/pControl cells, as determined by the amount of intracellular viral RNA following the viral infection (Figure 4D).

Silencing of *MX1* expression in Huh-7 cells increases their permissiveness for HCV replication.

We also determined whether knockdown of *MX1* expression in Huh-7 cells rendered these cells more permissive for HCV replication. For this purpose, we generated a line of Huh-7 cells (Huh-7/shMX1 cells) in which MX1 was knocked down by more than 90% by a stably transfected shRNA in cells treated with interferon (Figure 5A). Judging by the number of colonies that contained a transfected HCV subgenomic replicon, these cells were much more permissive for HCV replication than Huh-7 cells stably transfected with a control shRNA (Huh-7/shControl) but not so permissive as HRP4 cells (Figure 5B and

C). To determine the specificity of the shRNA-mediated knockdown of *MX1*, we stably transfected Huh-7/shMX1 cells with a plasmid overexpressing *MX1* to generate a line of cells (Huh-7/shMX1/pMX1) in which expression of *MX1* was restored to the level found in Huh-7 cells treated with interferon (Figure 5D). Restoration of *MX1* expression in Huh-7/shMX1 cells markedly reduced their permissiveness for HCV replication (Figure 5E and F).

_MX1_ is hypermethylated in HRP4 cells.

We then investigated the mechanism through which expression of *MX1* is suppressed in HRP4 cells. IFN-α was equally effective in activating a luciferase reporter gene driven by the 5′ flanking region of *MX1* in both Huh-7 and HRP4 cells (Figure 6A). This observation suggests that there is no defect in the interferon-stimulated signaling pathway leading to activation of *MX1* in HRP4 cells. We thus speculated that the defect must be in the *MX1* gene itself. Since we were unable to identify any mutations in the coding region or in the 5′ regulatory element of the gene in HRP4 cells, we suspected that the gene was epigenetically silenced in these cells. *MX1* was known to contain multiple CpG islands and silenced in several tumor cells through hypermethylation (Calmon et al., 2009; Desmond et al., 2007). We identified two cytosines in a CpG island located in the first intron of *MX1* that were methylated in HRP4 cells but not in their parental Huh-7 cells through bisulfite sequencing analysis (Figure 6B). While 5-azaC only slightly induced expression of*MX1* in Huh-7 cells treated with IFN-α (Figure 6C), the compound markedly raised the amount of *MX1* mRNA in interferon-treated HRP4 cells and completely restored its induction by IFN-α in these cells (Figure 6D).

DNA methylation profiles are different among subclones of Huh-7 cells.

Our results with HRP1 and HRP4 cells indicate that different anti-HCV genes are hypermethylated and silenced in different subclones of Huh-7 cells permissive for HCV replication: in HRP1 cells, *CREB3L1* is hypermethylated but expression of*MX1* is not affected, whereas in HRP4 cells, *MX1* is

hypermethylated but production of *CREB3L1* mRNA is only slightly reduced (Figure 2E). In contrast to these cells, neither gene is methylated in parental Huh-7 cells. These results suggest that genes methylated in these cells may be different. To test this hypothesis, we performed a methylated DNA microarray analysis (Weber et al., 2005). We immunoprecipitated methylated genomic DNA fragments with an antibody reacting against methylated cytosines and hybridized these fragments with probes covering all annotated promoters and CpG islands in the entire genome. The signal intensity of methylation of a specific segment of DNA was determined by its hybridization signal normalized against its input amount before immunoprecipitation. We then compared the global gene methylation profiles of two lines of cells by plotting their methylation signal intensities against each other. If two lines of cells shared a similar pattern in gene methylation, all dots in the plot should be closely fitted into a straight line, $y = x$. This was exactly the case when we compared gene methylation in HRP1 cells from two independent experiments (Figure 7A). This pattern was not observed when we compared gene methylation of Huh-7 and HRP1 cells (Figure 7B), Huh-7 and HRP4 cells (Figure 7C), or HRP1 and HRP4 cells (Figure 7D). Thus, the global gene methylation pattern is different among these cells.

Inasmuch as both HRP1 and HRP4 cells were selected from Huh-7 cells with an HCV subgenomic replicon, the above-mentioned results suggest that HCV infection may induce global changes in gene methylation in Huh-7 cells in an attempt to create a cellular environment more suitable for the virus to replicate. Alternatively, Huh-7 cells may exist as a heterogeneous population of cells with distinct patterns of gene methylation. This heterogeneity allows HCV to select a small population of the cells that have antiviral genes hypermethylated for replication. To test which one of these hypotheses was correct, rather than transfecting an HCV subgenomic replicon RNA carrying *neo*, we transfected Huh-7 cells with a plasmid carrying *neo* and selected two independent clones of the stably transfected cells (Huh-7/pNeo1 and Huh-7/pNeo2). Since these cells had never been infected by HCV, their gene methylation profiles were not expected to be different from that in Huh-7 cells if the alteration in gene methylation was induced by the virus. However, DNA methylation microarray analysis revealed that gene methylation

profiles in these cells were also different from those in Huh-7 (Figure 7E and F) and HRP4 (Figure 7G and H) cells. The gene methylation profiles of these two lines of cells were also different (Figure 7I). Thus, the difference in gene methylation among subclones of Huh-7 cells is most likely caused by epigenetic instability of Huh-7 cells that allows them to exist as a mixed population of cells with distinct gene methylation profiles.

2.5 Discussion

The current study reveals a critical role of gene methylation in generating subclones of Huh-7 cells permissive for HCV replication. We show that Huh-7 cells are a heterogeneous population of cells with distinct profiles in gene methylation. Most of these cells express genes that inhibit HCV replication so that they are resistant to the viral infection. A small number of the cells have certain anti-HCV genes hypermethylated and inactivated so that they are permissive for HCV replication. For example, *CREB3L1* and *MX1*, two anti-HCV genes, are silenced through gene methylation in our permissive subclones, HRP1 and HRP4 cells, respectively. Methylation of interferon-induced genes other than*MX1* has been reported to be responsible for generation of other subclones of Huh-7 cells permissive for HCV replication (Naka et al., 2006). This clonal variation in gene methylation may also explain why expression of so many genes is different between parental Huh-7 cells and subclones of Huh-7 cells permissive for HCV replication (Denard et al., 2011; Scholle et al., 2004). The difference among subclones of Huh-7 cells permissive for HCV replication may also explain conflicting results regarding host proteins that control HCV infection in the literature. One such example is MX1. In the current study, we demonstrate that MX1 plays an important role in inhibiting HCV replication by showing that cells deficient in MX1 were permissive for HCV replication and that restoration of MX1 expression in these cells abolished their ability to support HCV replication. However, a previous study showed that overexpression of MX1 failed to inhibit HCV replication (Frese et al., 2001). The most likely explanation for the discrepancy is that there was no defect in MX1 expression in subclones of Huh-7 cells harboring the HCV replicon in the earlier study (Frese et al., 2001). These results suggest that while silencing *MX1* makes Huh-7 cells more permissive for HCV replication, overexpression of *MX1* in cells already expressing normal amounts of the protein may not necessarily make the cells more resistant to HCV infection. Thus, identifying the mechanism through which subclones of Huh-7 cells become permissive for HCV replication is crucial for understanding their interaction with HCV.

An important observation in the current study is that HRP4 cells also express much less CREB3L1

protein than their parental Huh-7 cells. This result reaffirms our previous conclusion that CREB3L1 plays a critical role in limiting HCV replication in Huh-7-derived cells. While both HRP1 and HRP4 cells express very little CREB3L1 protein, the amount of CREB3L1 mRNA is much higher in HRP4 cells than in HRP1 cells. This result suggests that epigenetic silencing of CREB3L1 observed in HRP1 cells is unlikely to be the mechanism through which CREB3L1 expression is inhibited in HRP4 cells. Instead, the result suggests that CREB3L1 expression is inhibited at a posttranscriptional step in HRP4 cells. Identification of the mechanism through which CREB3L1 expression is inhibited in HRP4 cells may reveal novel pathways that regulate this antiviral factor.

2.6 Chapter Two Figures

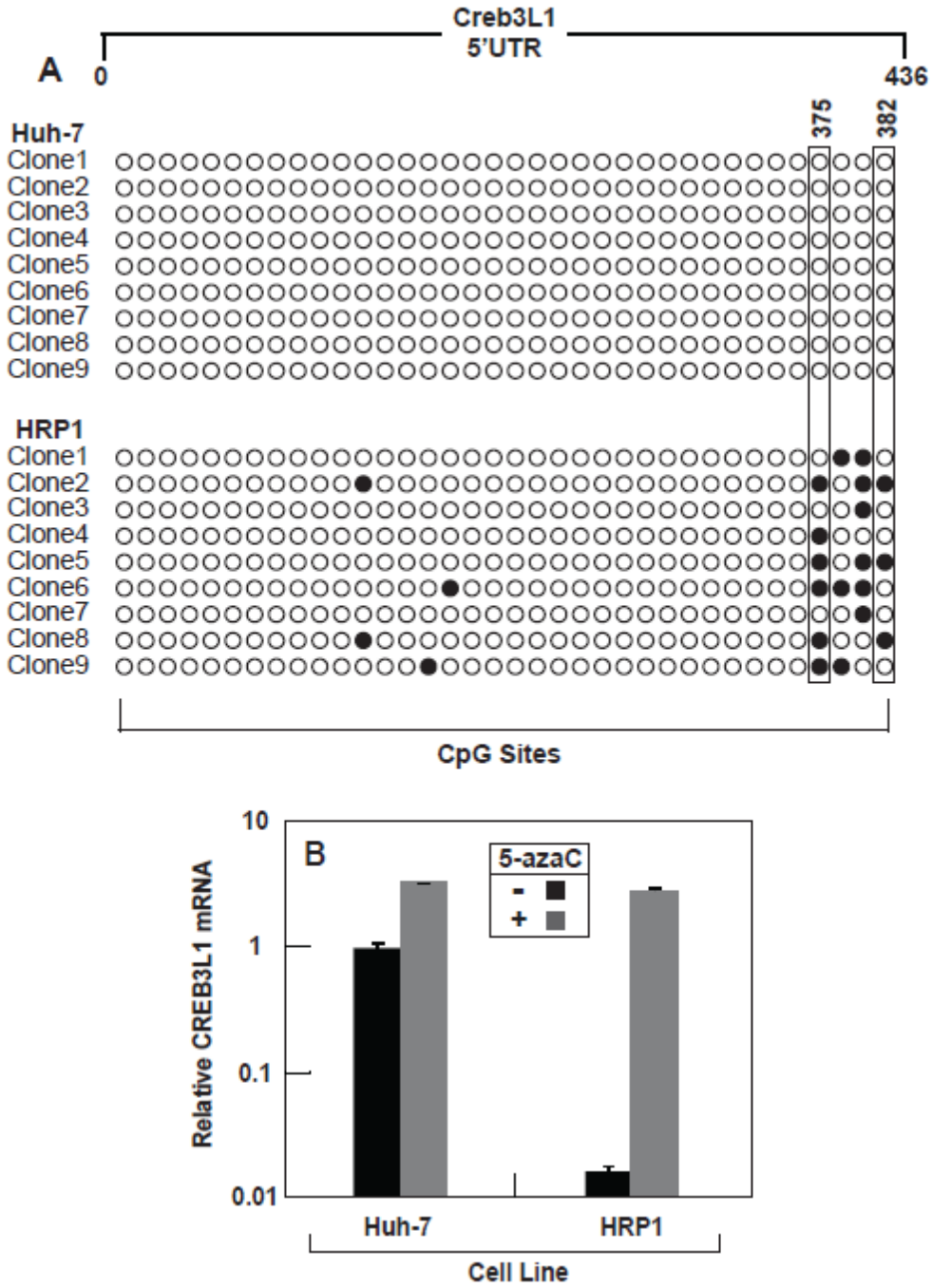

Figure 1. CREB3L1 is hypermethylated in HRP1 cells.
(A) On day 0, indicated cells were seeded at 4×10^5/60-mm dish. On day 1, cells were harvested and genomic DNA was extracted for bisulfite sequencing as described in Materials and Methods. The closed and open circles denote methylated and unmethylated CpGs, respectively. The position is numbered according to the transcriptional initiation site, which is set at 1. Cytosines that were not methylated in Huh-7 cells but methylated in more than 50% of PCR clones amplified from HRP4 cells are boxed.

(B) On day 0, indicated cells were seeded at 4×10^5/60-mm dish. On day 1, cells were treated with 30 μM 5-azaC. On day 4, cells were harvested, and the amount of CREB3L1 mRNA was quantified by RT-qPCR, with the value in Huh-7 cells untreated with 5-azaC set to 1. Results are reported as means and standard deviations (SDs) from three independent experiments.

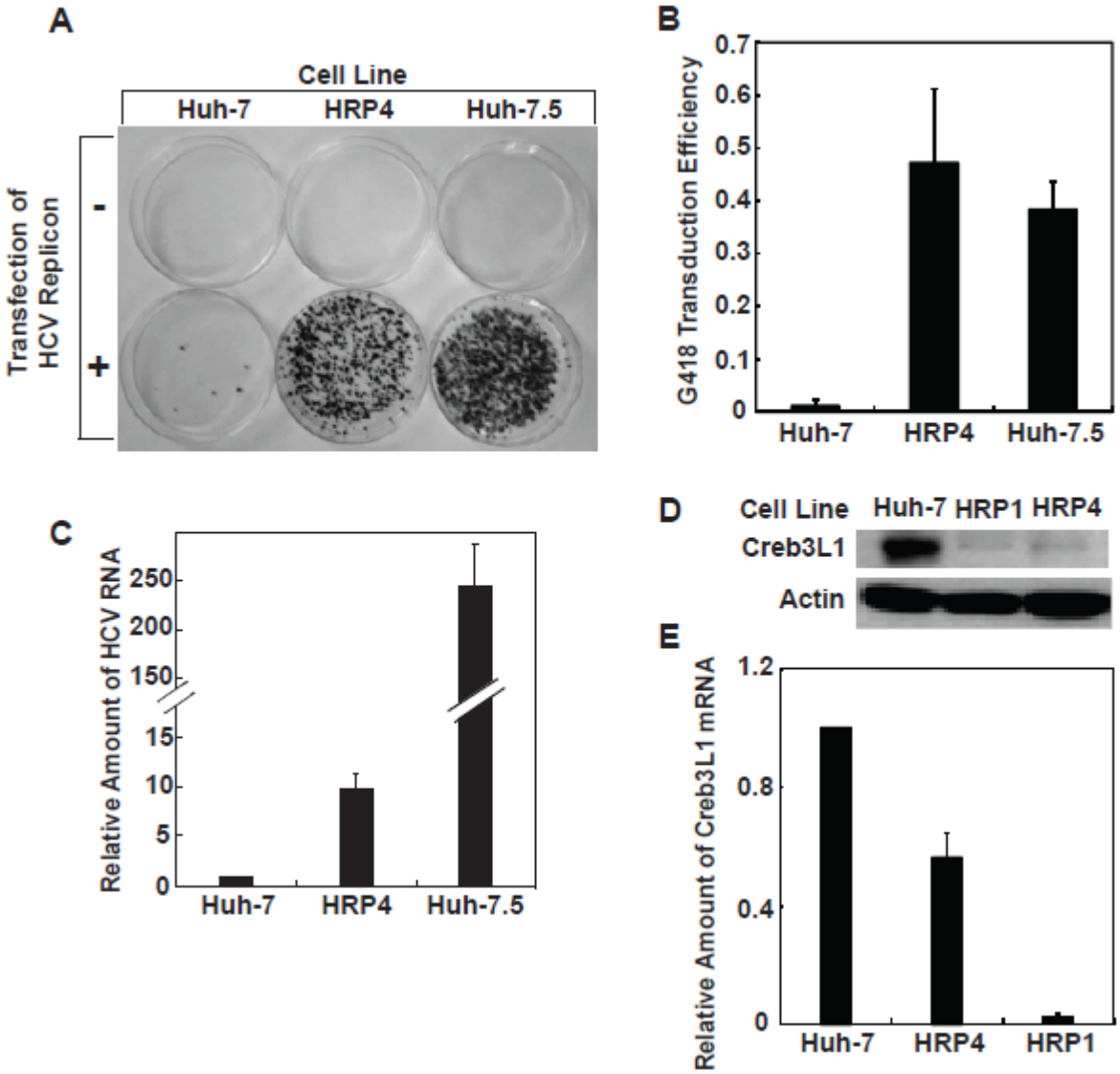

Figure 2. HRP4 cells are permissive for HCV replication.
(A and B) On day 0, the indicated cells were seeded at 7×10^5/60-mm dish. On day 1, cells were transfected with an HCV replicon (HP; 0.5 μg/dish). On day 3, cells were treated with 700 μg/ml G418. After 2 weeks of G418 selection, the cells were stained with crystal violet. A representative picture of the staining result (A) and quantification of G418 transduction efficiency (B) are presented.
(C) On day 0, the indicated cells were seeded at 7×10^5/60-mm dish. On day 1, cells were infected with the JFH-1 strain of HCV. On day 5, cells were harvested, and the amount of intracellular HCV RNA was quantified by RT-qPCR, with the value in Huh-7 cells set at 1.
(D) Quantification of the CREB3L1 protein in indicated cells by immunoblot analysis.
(E) Quantification of CREB3L1 mRNA in indicated cells by RT-qPCR, with the value in Huh-7 cells set at 1.
(B, C, and E) Results are reported as means and SDs from three independent experiments.

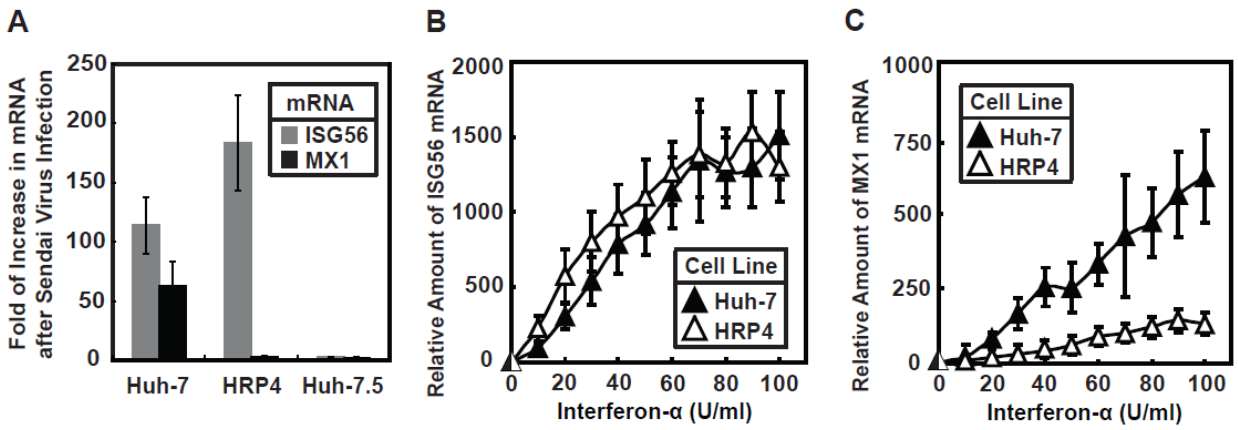

Figure 3. HRP4 cells are defective in inducing MX1 expression in response to interferon.
(A) On day 0, indicated cells were seeded at 4×10^5/60-mm dish. On day 1, some of these cells were infected by Sendai virus. On day 2, cells were harvested and the indicated mRNA was determined by RT-qPCR. Fold induction of the indicated mRNA by Sendai virus infection is presented.
(B and C) On day 0, indicated cells were seeded at 4×10^5/60-mm dish. On day 1, cells were treated with the indicated concentration of alpha interferon for 6 h. Cells were harvested, and the amount of ISG56 (B) and MX1 (C) mRNA was quantified by RT-qPCR, with the value in untreated HRP4 cells set at 1.
(A to C) Results are reported as means and SDs from three independent experiments.

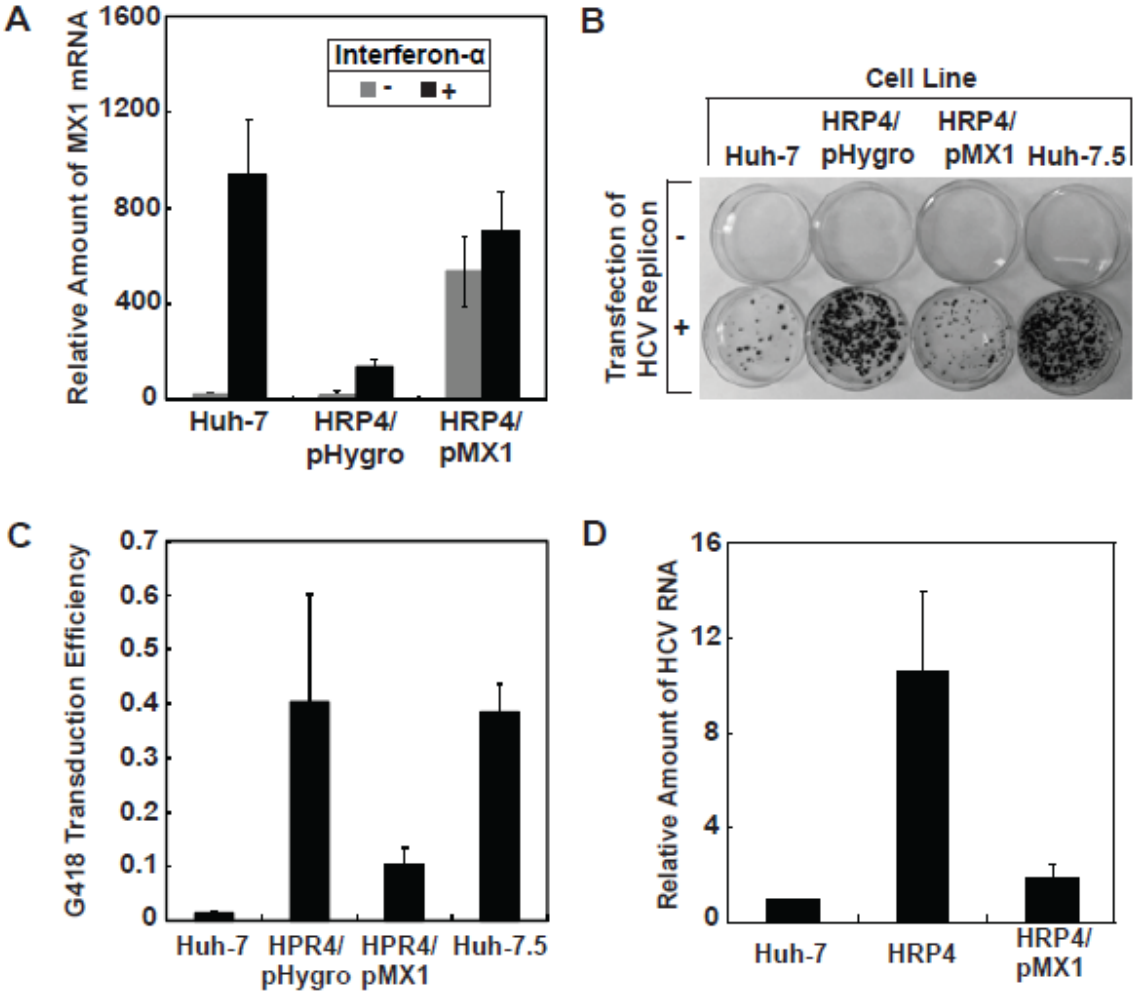

Figure 4. Restoration of MX1 expression reduces the permissiveness of HRP4 cells for HCV replication.

(A) On day 0, indicated cells were seeded at 7×10^5/60-mm dish. On day 1, cells were treated with 100 U/ml of alpha interferon for 6 h. The amount of MX1 mRNA was quantified by RT-qPCR, with the value in untreated Huh-7 cells set at 1.

(B and C) On day 0, indicated cells were seeded at 7×10^5/60-mm dish. The indicated cells transfected with the HCV replicon were selected by G418, stained with crystal violet, and analyzed as described in Figure 2A and B

(D) On day 0, indicated cells were seeded at 7×10^5/60-mm dish. The indicated cells were infected with the JFH-1 strain of HCV and analyzed as described in Figure 2C.

(A to D) Bar graphs show the means and SDs from three independent experiments.

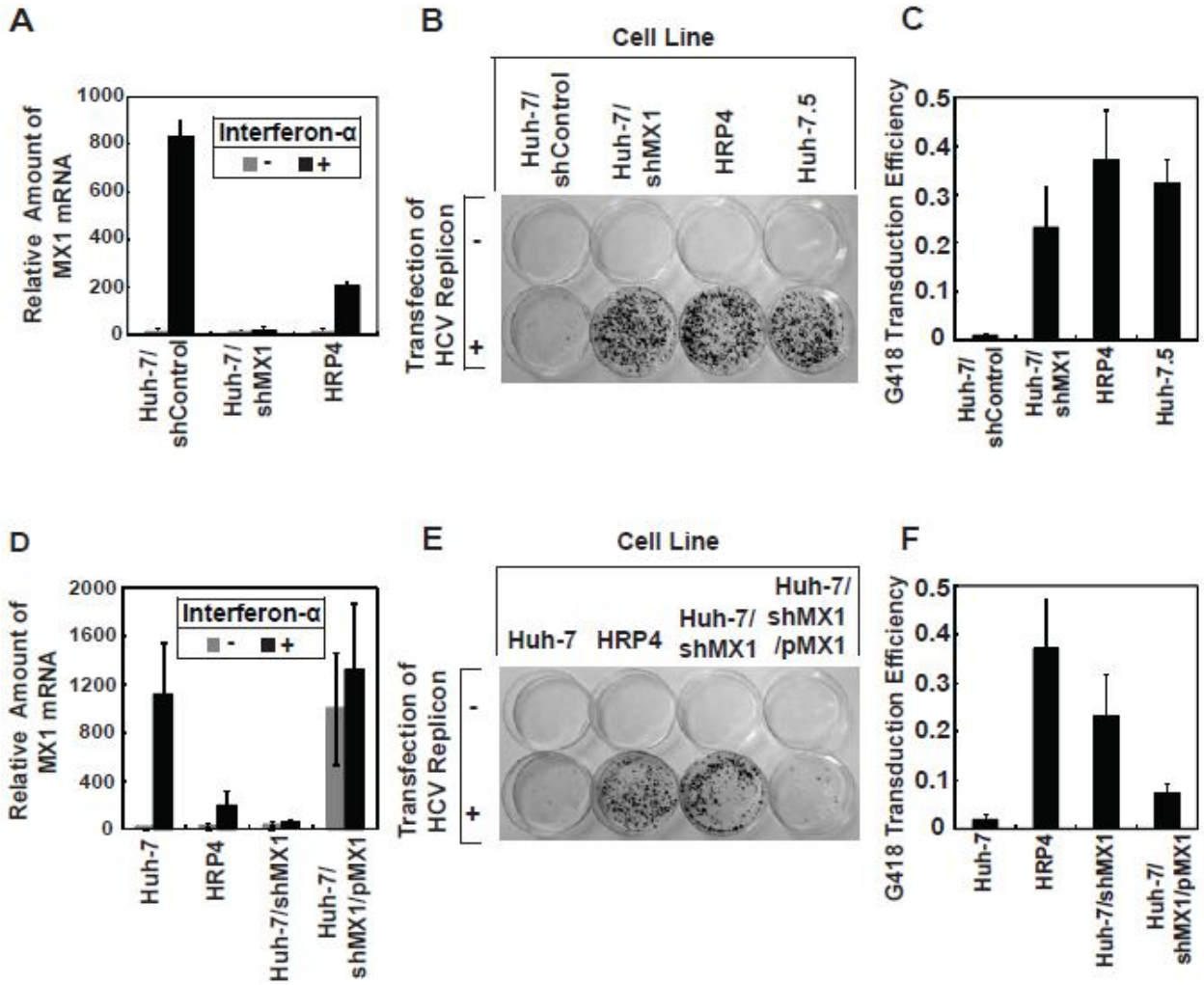

Figure 5. Silencing of *MX1* expression in Huh-7 cells increases their permissiveness for HCV replication.

(A and D) Quantification of MX1 mRNA was performed as described in Figure 4A, with the value in untreated Huh-7/shControl (A) or Huh-7 (D) cells set at 1.

(B, C, E, and F) The indicated cells transfected with the HCV replicon were selected by G418, stained with crystal violet, and analyzed as described in Figure 2A and B.

(A to F) Bar graphs show the means and SDs from three independent experiments.

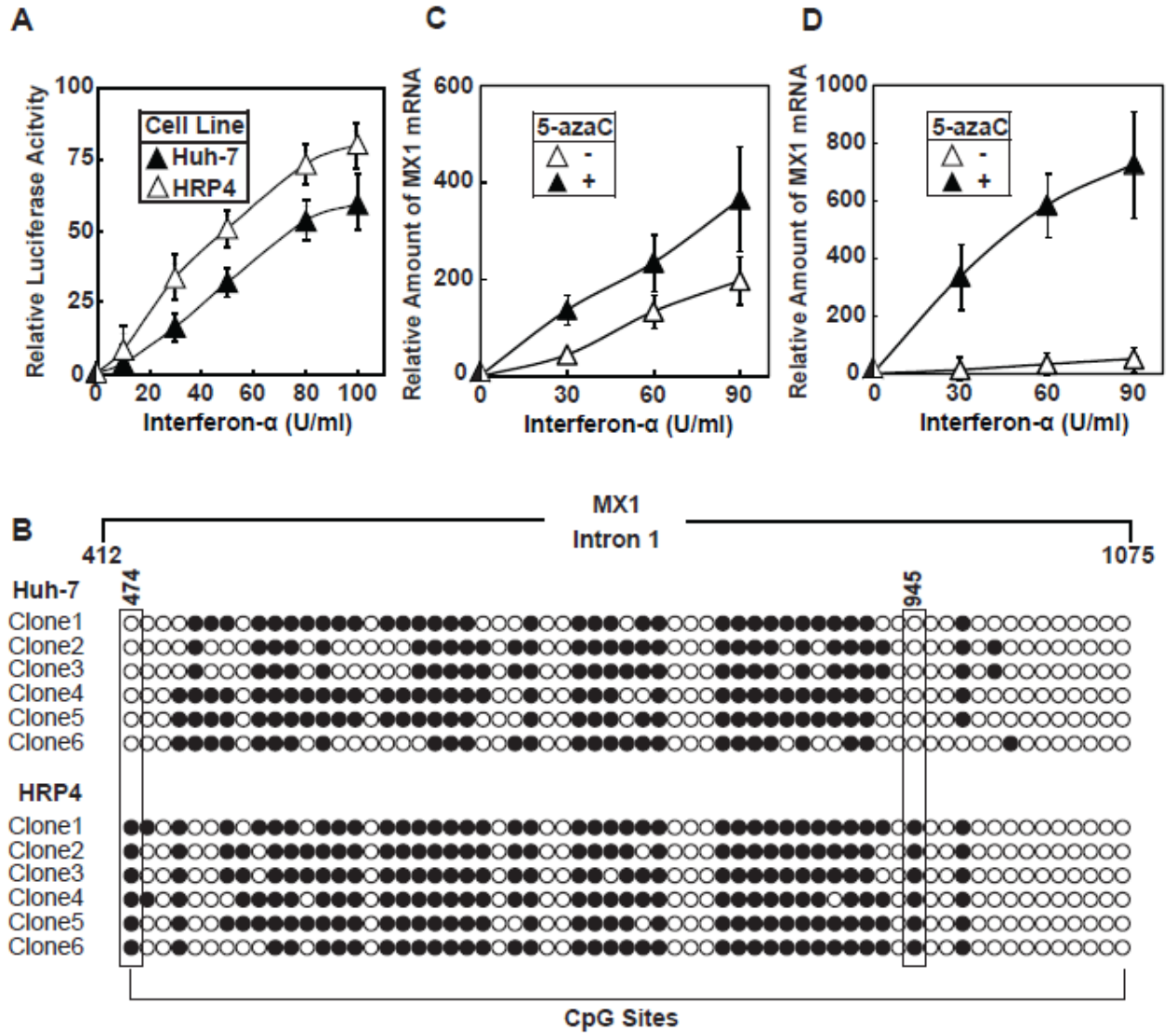

Figure 6. *MX1* is hypermethylated in HRP4 cells.
(A) On day 0, indicated cells were seeded at 7×10^5cells/60-mm dish. On day 1, cells were transfected with a firefly luciferase reporter plasmid driven by the MX1 promoter (1 μg/dish) and a plasmid encoding *Renilla* luciferase that was driven by the constitutive cytomegalovirus (CMV) promoter (0.5 μg/dish). On day 2, cells were treated with the indicated amount of alpha interferon for 6 h. Luciferase activity was measured, and the promoter activity was determined by firefly luciferase activity normalized against *Renilla* luciferase activity to control for transfection efficiency. Results are the means and SDs from triplicate incubations of a representative experiment.
(B) Methylation of CpG sites in the first intron of MX1 was analyzed as described in Figure 1A.
(C and D) On day 0, indicated cells were seeded at 7×10^5cells/60-mm dish. On day 0, indicated cells were seeded at 7×10^5cells/60-mm dish. On day 1, Huh-7 (C) and HRP4 (D) cells were treated with 4 μM 5-azaC or untreated. On day 4, cells were treated with the indicated concentration of alpha interferon for 6 h. The amount of MX1 mRNA in these cells was quantified by RT-qPCR, with the value in Huh-7 cells untreated with either interferon or 5-azaC set at 1. Results are the means and SDs from three independent experiments.

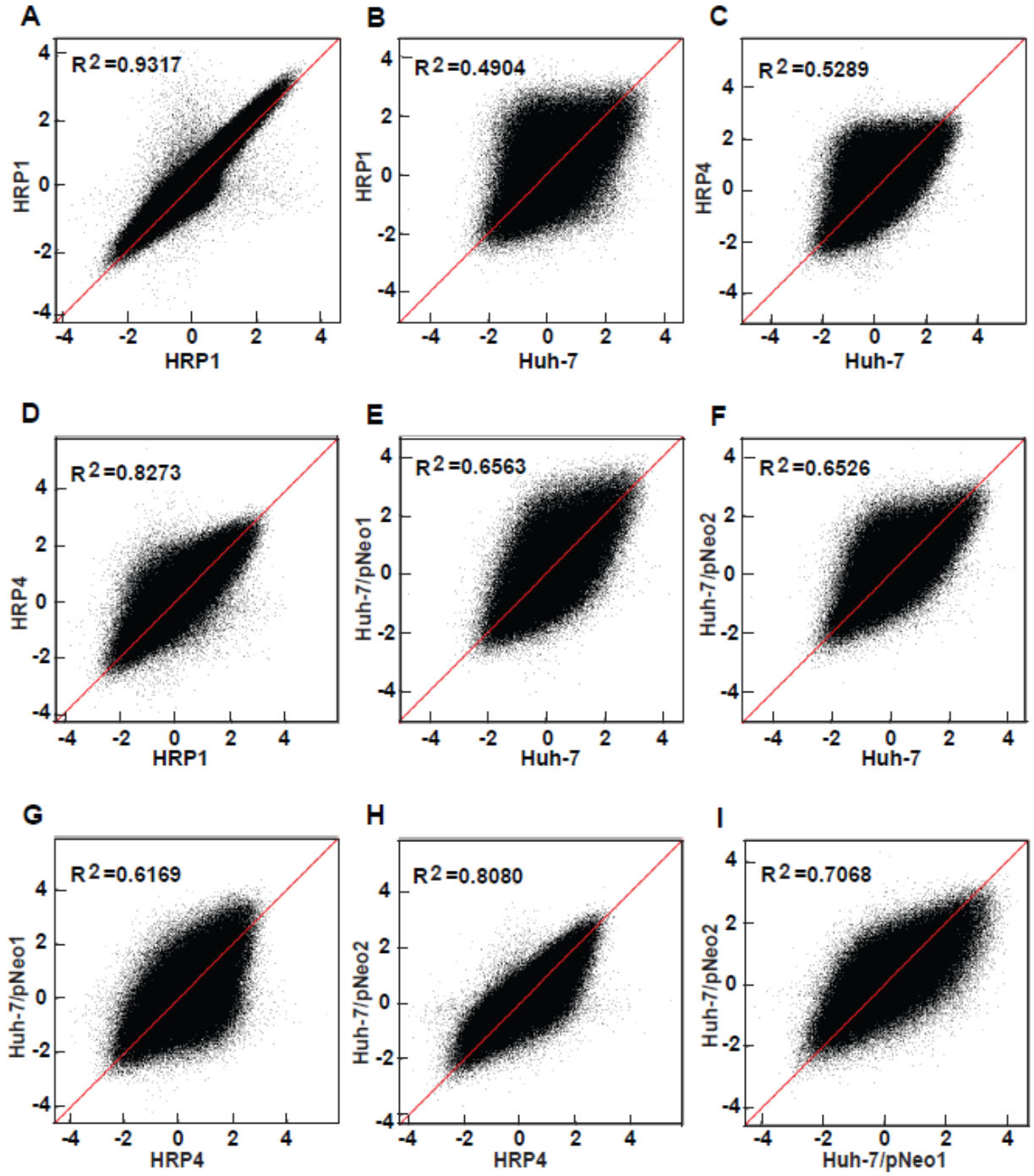

Figure 7. DNA methylation profiles are different among subclones of Huh-7 cells.

(A-I) The DNA methylation microarray was performed as described in Materials and Methods. The coordinates of each point show the signal intensity of methylation of a specific segment of DNA in cells indicated on the *x* and *y* axes. The diagonal line $y = x$ is highlighted in red. The R^2 value for each comparison is presented.

CHAPTER THREE:

Sbustained Induction of Collagen Synthesis by TGF-β Requires Regulated Intramembrane Proteolysis of CREB3L1

3.1 Abstract

Transforming growth factor-β (TGF-β) induces excessive synthesis of collagen causing tissue fibrosis, but the underlying mechanism remains elusive. Here we show that sustained induction of collagen synthesis by TGF-β requires proteolytic activation of cAMP response element binding protein 3-like 1 (CREB3L1), a transcription factor synthesized as a membrane-bound precursor and activated through Regulated Intramembrane Proteolysis (RIP). RIP of CREB3L1 is inhibited by transmembrane 4 L6 family member 20 (TM4SF20), which retains CREB3L1 in the endoplasmic reticulum thereby separating CREB3L1 from the Golgi-resident proteases catalyzing the RIP reaction. TGF-β inhibits TM4SF20 expression through activation of extracellular signal-regulated kinases to stimulate RIP of CREB3L1. This cleavage allows the NH_2-terminal fragment of CREB3L1 to enter the nucleus where it forms a complex with Smad4 to activate transcription of genes involved in assembly of collagen extracellular matrix. Our study suggests that RIP of CREB3L1 could be a drug target to treat tissue fibrosis.

3.2 Introduction

Excessive deposition of collagen to tissue surface results in tissue fibrosis, a pathological condition that often leads to tissue dysfunction and organ failure(Rosenbloom et al., 2010).. Transforming growth factor-β (TGF-β) has been identified as a key factor that induces epithelial to mesenchymal transition (EMT), a process believed to be crucial for activating collagen synthesis in fibrotic tissues (Gordon and Blobe, 2008; Nieto, 2011; Verrecchia and Mauviel, 2007). TGF-β initiates the signaling cascade by binding to its cell surface receptor, which in turn phosphorylates Smad2 and Smad3, the receptor-activated Smad proteins (Massague, 2012). Phosphorylated Smad2 or Smad3 forms a complex with the common Smad protein Smad4 (Massague, 2012). This complex translocates to nucleus where it activates its target genes including those required for assembly of collagen extracellular matrix (Burch et al., 2011; Doyle et al., 2012; Massague, 2012). This mechanism, however, only accounts for acute induction of collagen synthesis by TGF-β, because the cytokine-induced activation of Smad2 or Smad3 through phosphorylation is a transient event (Massague, 2012). The mechanism through which TGF-β induces chronic accumulation of collagen, a condition more related to fibrotic development, has yet been identified.

In addition to the Smad-dependent pathway, TGF-β also activates Smad-independent non-canonical pathways, which include activation of extracellular signal-regulated kinases (ERKs) (Derynck and Zhang, 2003). ERK activation has been reported to play a critical role in TGF-β-induced pathological events (Holm et al., 2011). However, the contribution of ERK activation on TGF-β-induced collagen synthesis and fibrotic diseases has yet to be determined.

Recent studies have identified cAMP response element binding protein 3-like 1 (CREB3L1, also known as OASIS) as a transcription factor that activates genes involved in assembly of collagen extracellular matrix (Denard et al., 2011; Murakami et al., 2009). CREB3L1 belongs to a family of transcription factors synthesized as transmembrane precursors (Omori et al., 2002) and activated through

a process designated as Regulated Intramembrane Proteolysis (RIP) (Brown et al., 2000). CREB3L1 contains a single transmembrane domain with the NH_2-terminal transcription factor domain projecting into the cytosol and a COOH-terminal domain projecting into the lumen of the endoplasmic reticulum (ER). Viral infection, ER stress or chemotherapeutic reagent doxorubicin triggers the RIP of CREB3L1, which undergoes two sequential cleavages catalyzed by Site-1 protease (S1P) and Site-2 protease (S2P) (Denard et al., 2012; Denard et al., 2011; Murakami et al., 2006), two proteases localized in the Golgi complex (DeBose-Boyd et al., 1999). The S1P-catalyzed cleavage at the luminal side is a prerequisite for the S2P-catalyzed intramembrane cleavage that releases the NH_2-terminal domain of the protein from membranes, allowing it to enter nucleus where it drives transcription of genes required for assembly of collagen extracellular matrix (Denard et al., 2012; Denard et al., 2011; Murakami et al., 2006). Exactly how these stimulus trigger RIP of CREB3L1 remains unclear.

In contrast to CREB3L1, the mechanism through which sterol deprivation stimulates RIP of sterol regulatory element binding proteins (SREBPs), a prototype of RIP substrates, has been identified (Brown and Goldstein, 2009). In cells loaded with sterols, SREBPs are retained in the ER through their interaction with the Insig proteins (Yabe et al., 2002; Yang et al., 2002). As a result, SREBPs are not cleaved because they are separated from Golgi-localized S1P and S2P (DeBose-Boyd et al., 1999). Sterol depletion disrupts the interaction between Insig proteins and SREBPs (Yabe et al., 2002; Yang et al., 2002), thereby stimulating transport of SREBPs from the ER to Golgi where SREBPs are cleaved by S1P and S2P (DeBose-Boyd et al., 1999; Nohturfft et al., 2000). Similarly, activation transcription factor 6 (ATF6), another RIP substrate, is retained in the ER through its interaction with Bip (Shen et al., 2002). ER stress leads to dissociation of ATF6 from Bip, thereby stimulating transport of ATF6 from the ER to Golgi where it is cleaved by S1P and S2P (Shen et al., 2002; Ye et al., 2000). In contrast to these well-characterized RIP reactions, the protein that retains CREB3L1 in the ER has not been identified.

In the current study, we determine that TGF-β stimulates RIP of CREB3L1, and this proteolytic activation is required for prolonged activation of genes involved in assembly of collagen extracellular matrix. We further demonstrate that transmembrane 4 L6 family member 20 (TM4SF20), a membrane protein without a previously identified function, plays an important role in TGF-β-induced RIP of CREB3L1. We show that CREB3L1 is retained in the ER through its interaction with TM4SF20, and TGF-β stimulates RIP of CREB3L1 by inhibiting expression of TM4SF20 through an ERK-dependent pathway. These results suggest that the signaling pathway leading to activation of CREB3L1 could be targeted by drugs to treat fibrotic diseases.

3.3 Material and Methods

Materials

We obtained RDEA119 from ChemieTek (Indianapolis, IN); mouse anti-phospho-ERK from Sigma (St, Louis, MO); rabbit anti-LSD1 from Cell Signaling (Boston, MA); mouse anti-calnexin from Enzo Life Sciences (Farmingdale, NY); mouse anti-Smad4 and rabbit anti-ERK from Santa Cruz Biotechnology (Santa Cruz, CA); mouse anti-Smad2, mouse anti-phospho-Smad2, mouse anti Smad3, and mouse anti-phospho-Smad3 from Cell Signaling Technology (Danvers, MA); peroxidase-conjugated secondary antibodies, Alexa 488 and CY3 conjugated secondary antibodies from Jackson ImmunoResearch (West Grove, PA); TGF-β1 from R&D (Minneapolis, MN). Hybridoma cells producing IgG-9E10, a mouse monoclonal antibody against Myc tag, were obtained from the American Type Culture Collection (Manassas, VA). A rabbit polyclonal antibody against human CREB3L1 was generated as previously described (Denard et al., 2011).

Plasmid

pCMV-TM4SF20-$(Myc)_5$ encodes full length human TM4SF20 followed by 5 tandem repeats of the myc epitope tag. It is produced by ligating BamHI and NheI-cleaved vector pcDNA3.1-$(Myc)_5$ (Wang et al., 2005)with the PCR product corresponding to full length TM4SF20.

Cell culture

A549 cells were maintained in medium A (1:1 mixture of Ham's F12 medium and Dulbecco's modified Eagle's medium containing 100 U/ml penicillin and 100 μg/ml streptomycin sulfate supplemented with 5% [vol/vol] fetal calf serum (FCS)). A549/pTM4SF20 cells were generated by transfecting pCMV-TM4SF20-$(Myc)_5$ followed by selection with 700 μg/ml G418. The cells were maintained in medium A supplemented with 700 μg/ml G418. Huh7 cells were maintained in medium B (Dulbecco's modified

Eagle's medium with 4.5 g/l glucose, 100 U/ml penicillin, 100 mg/ml streptomycin sulfate, and 10% [vol/vol] FCS). A549-derived cells were cultured in monolayers at 37°C in 8.8% CO_2, whereas Huh7 cells were maintained at 37°C in 5% CO_2.

Immunoblot analyses

Cells were harvested and separated into nuclear and membrane fractions as described (Sakai et al., 1996), and analyzed by SDS-PAGE followed by immunoblot analysis with the indicated antibodies (1:4000 dilution for anti-calnexin, 1:2000 dilution for anti-Myc, anti-CREB3L anti-ERKs and anti-phospho-ERKs, and 1:1000 dilution for the rest of the antibodies). Bound antibodies were visualized with a peroxidase-conjugated secondary antibody using the SuperSignal ECL-HRP substrate system (Pierce).

RNA interference

Duplexes of siRNA were synthesized by Dharmacon Research. The two siRNA sequences targeting human CREB3L1 are CGGAGAACAUGGAGGACUU and CCACCAAGUACCUGAGUGA. The two siRNA sequences targeting human Smad4 are GAUUAACACUGCAGAGUAA and GCAAUUGAAAGUUUGGUAA. The two siRNA sequences targeting human TM4SF20 are GCGAGUGGCUGGAGAGCAU and GUCUAUUGCUUGUUGGAAU. The control siRNA targeting GFP was reported previously (Adams et al., 2004). Cells were transfected with siRNA using Lipofectamine RNAiMAX reagent (Invitrogen) as described by the manufacturer, after which the cells were used for experiments as described in the figure legends.

RT-QPCR

RT-QPCR was performed as previously described (Liang et al., 2002). Each measurement was made in triplicate from cell extracts pooled from duplicate dishes. The relative amounts of RNAs were calculated through the comparative cycle threshold method by using human 36B4 mRNA as the invariant control.

Immunoprecipitation

For co-immunoprecipitation of Smad4 and CREB3L1, pooled cell pellets from 5 dishes of indicated cells were resuspended in 0.4 ml of buffer A (25 mM Tris-HCl pH 7.2, 0.15 M NaCl, 1% Nonidet P-40, 5 μg/ml pepstatin, 10 μg/ml leupeptin, 2 μg/ml aprotinin, 2 μg/ml N-[N-(N-Acetyl-L-leucyl)-L-leucyl]-L-norleucine). Cell lysates were rotated at 4 °C for 1 h and clarified by centrifugation at 20,000 × *g* for 10 min. The lysates were pre-cleared by incubation for 30 min at 4°C with 50 μl of Protein A/G agarose beads (Santa Cruz Biotechnology). The pre-cleared lysates were rotated for 16 h at 4°C with 15 μg of polyclonal anti-CREB3L1 or control IgG together with 50 μl of protein A/G agarose beads. After centrifugation at 200 × *g* for 5 min, the resulting supernatants were collected. The pelleted beads were washed for three times (10 min each time at 4°C) with 0.7 ml of buffer A, followed by suspension in 100 μl Laemmli sample buffer dissolved in buffer A. Immunoprecipitated material was eluted by boiling and collected following centrifugation. Supernatant and pellet fractions were then subjected to SDS/PAGE followed by immunoblot analysis. The same procedure was applied to co-immunoprecipitation of TM4SF20 and CREB3L1, except that 1% (w/v) digitonin instead of 1% Nonidet P-40 was used in the experiment.

Microarray Analysis

Microarray analysis was performed exactly as previously described (Horton et al., 2003). The result was deposited at Gene Expression Omnibus (GEO) with accession number GSE46024.

Immunofluorescent Microscopy

Cells gown on cover slips were fixed in 1 ml 4% paraformaldehyde for 10 min at room temperature. The cells were then permeabilized in methanol overnight at -20˚C, rehydrated in 0.1M phosphate buffer saline (PBS) for 10 min at room temperature, blocked in 0.1 M PBS containing 1% BSA for 1 h at room temperature, and incubated with primary antibodies (1:500 for anti-Myc, 1:1000 for anti-calnexin)

overnight at 4˚C. After washing three times (10 min each time at room temperature) with 0.1M PBS, the cover slips were incubated with secondary antibodies (1:500 dilutions) and DAPI (100ng/ml) for 2 h in the dark at room temperature. They were then washed, sealed and observed under a Zeiss LSN 510 fluorescent confocal microscope.

Xbp1 splicing

Cells were harvested and RNA was extracted using the RNeasy Kit from Qiagen (Germantown, MD). First-strand cDNA was synthesized from the DNA-free RNA by using random hexamer primers and the ABI cDNA synthesis kit (Applied Biosystems, Grand Island, NY). Forward primer AAACAGAGTAGCAGCTCAGACTGC and reverse primer TCCTTCTGGGTAGACCTCTGGGAG were used to amplify XBP1 cDNA. Amplified products were separated on a 2% agarose gel and visualized under UV light.

Ceramide measurement

Cells pooled from six 100-mm dishes were harvested for measurement of ceramide content by LC-MS analyses performed by UPLC-MS/MS at UT Southwestern Medical Center Mouse Metabolic Phenotyping Core exactly as previously described (Denard et al., 2012).

3.4 Results

Sustained activation of collagen synthesis requires RIP of CREB3L1

We used A549 cells that have been established as a model system to study the effect of TGF-β on EMT (Kasai et al., 2005; Zavadil and Bottinger, 2005) to determine the effect of the cytokine on RIP of CREB3L1. For this purpose, we fractionated A549 cells into nuclear and membrane fractions, and used an antibody reacting against the NH_2-terminal domain of CREB3L1 to examine the cleavage of CREB3L1 through immunoblot analysis. In the absence of TGF-β, CREB3L1 existed as the full length precursor (~80 kDa) in membranes and the cleaved nuclear form of CREB3L1 (~55 kDa) was undetectable (Figure 8A, lane 1). The cleaved nuclear form appeared 8 h after the treatment with TGF-β, and its amount gradually increased with longer treatment up to 24 h (Figure 8A, lanes 6-8). This cleavage was maintained in cells treated with TGF-β for 3 days (Figure 8B). This slow but sustained response of TGF-β was in sharp contrast with TGF-β-stimulated phosphorylation of Smad2 and Smad3: Both proteins were phosphorylated within 1 h of the TGF-β treatment, but the phosphorylation was no longer detectable 4 h after the treatment (Figure 8C).

To determine the effect of CREB3L1 activation on TGF-β-induced transcription of genes involved in assembly of collagen matrix, we transfected cells with two duplexes of siRNA targeting different regions of CREB3L1 that knocked down expression of CREB3L1 by ~80% and 60%, respectively (Figure 9A). Consistent with the observation that TGF-β-induced RIP of CREB3L1 is a late response for the cytokine, knockdown of CREB3L1 expression by the siRNA only slightly inhibited activation of *collagen 1α1* (*COL1A1*) transcription during the first 8 h of the treatment with TGF-β (Figure 9B). While longer treatment with TGF-β further raised the amount of COL1A1 mRNA in cells transfected with the control siRNA (Figures 9B and C, black line), such increase was blocked in cells transfected with the siRNA targeting CREB3L1 (Figures 9B and C, red and blue lines). Knockdown of CREB3L1 also blocked TGF-β-activated transcription of *secreted protein acidic and rich in cysteine* (*SPARC*), a target gene of

CREB3L1 (Denard et al., 2011) encoding a protein required for assembly of collagen extracellular matrix (Martinek et al., 2007) (Figure 9D). In contrast, TGF-β-mediated activation of *fibronectin* and suppression of *E-cadherin* transcription, two well known markers for EMT induced by TGF-β (Nieto, 2011), were not inhibited by knockdown of CREB3L1 (Figures 9E and F). In fact, knockdown of CREB3L1 slightly increased the amount of fibronectin mRNA in response to TGF-β treatment (Figure 9E). These results suggest that CREB3L1 is specifically required for TGF-β to activate genes involved in assembly of collagen extracellular matrix.

Nuclear CREB3L1 forms a complex with Smad4 to activate target genes.

We then determined the relationship between signal transduction mediated by Smad proteins and RIP of CREB3L1. For this purpose, we transfected cells with two duplexes of siRNA targeting different regions of Smad4, the common Smad protein that is required for both Smad2 and Smad3 to regulate transcription of their target genes (Massague, 2012). Such treatment knocked down expression of Smad4 by more than 80% (Figure 10A). Surprisingly, knockdown of Smad4 had no effect on TGF-β-induced cleavage of CREB3L1 (Figure 10B), even though it completely blocked TGF-β-activated transcription of *COL1A1* and *SPARC* (Figures 10C and D). These results suggest that in the absence of Smad4, nuclear CREB3L1 is unable to activate its target genes. A likely explanation for the observation is that Smad4 could bind to nuclear CREB3L1 to serve as a transcriptional co-activator to stimulate transcription of genes activated by nuclear CREB3L1. To test this hypothesis, we performed a co-immunoprecipitation experiment to determine whether Smad4 forms a complex with nuclear CREB3L1. We immunoprecipitated nuclear CREB3L1 with an antibody against the protein. Nearly all nuclear CREB3L1 was precipitated by this antibody because the protein was depleted from the supernatant fraction of the immunoprecipitation carried out by anti-CREB3L1 but not a control antibody (Figure 10E, the lower panel). We were unable to show nuclear CREB3L1 in the immunoprecipitates because the protein co-migrated with the heavy chain of IgG. Smad4 was only found in the pellet fraction of

immunoprecipitation carried out by anti-CREB3L1 in lysate of cells treated with TGF-β (Figure 10E, lane 4, upper panel), which stimulated production of nuclear CREB3L1 (Figure 10E, lane 2, lower panel). This result suggests that Smad4 is in complex with nuclear CREB3L1.

To further determine the role of Smad4 on transcriptional activity of nuclear CREB3L1, we examined the requirement of Smad4 on doxorubicin-induced transcription of *COL1A1*, a reaction known to be driven by nuclear CREB3L1(Denard et al., 2012). For this purpose, we knocked down Smad4 in Huh7 cells by siRNA (Figure 10F). Knockdown of Smad4 did not affect doxorubicin-induced RIP of CREB3L1 (Figure 10G) but it significantly inhibited doxorubicin-induced synthesis of COL1A1 mRNA (Figure 10H). Thus, Smad4 appears to be a co-activator for nuclear CREB3L1 to induce transcription of *COL1A1* in multiple systems.

TGF-β induces RIP of CREB3L1 by inhibiting expression of TM4SF20

We then determined the mechanism through which TGF-β induces RIP of CREB3L1. Previous studies showed that ER stress triggered RIP of CREB3L1 (Murakami et al., 2006; Murakami et al., 2009). However, ER stress does not appear to be involved in TGF-β-induced cleavage of CREB3L1, as TGF-β did not induce splicing of XBP-1 (Figure 11A), a marker for ER stress (Walter and Ron, 2011). Our previous work demonstrated that doxorubicin stimulated RIP of CREB3L1 through activation of ceramide synthesis (Denard et al., 2012). Nevertheless, mass spectroscopy analysis indicated that TGF-β did not enhance production of ceramide (Figure 11B), an observation suggesting that increased ceramide synthesis is also not responsible for TGF-β-induced cleavage of CREB3L1.

Since it took 12 h for TGF-β to induce significant cleavage of CREB3L1 (Figure 8A), we suspected that TGF-β may induce RIP of CREB3L1 by regulating expression of certain genes. Microarray analysis revealed that TGF-β altered expression of 25 genes by more than 5 folds during this period of time (Table 2). Since proteins regulating cleavage of SREBPs, the best studied RIP substrates, are all transmembrane proteins (Brown and Goldstein, 2009), we hypothesized that the protein regulating cleavage of CREB3L1

may be a transmembrane protein as well. Among the 25 genes in the list, 5 of them encoded proteins known or predicted to be transmembrane proteins according to the gene database in the National Center for Biotechnology Information (NCBI) (Table 2). Among these proteins, claudin 4 (CLDN4), cholinergic receptor nicotinic α9 (CHRNA9), and ADAM metallopeptidase domain 19 (ADAM19) are known to be located and functioning in plasma membranes (Kang et al., 2002; Nguyen et al., 2000; Tsukita and Furuse, 2002). Since previous studies demonstrated that membrane proteins localized in the ER and Golgi regulated RIP of SREBPs by controlling transport of SREBPs from the ER to Golgi (Brown and Goldstein, 2009), we believe that these plasma membrane proteins are unlikely to be involved in regulating RIP of CREB3L1. We thus focused our attention on the remaining 2 genes, namely leucine rich repeat containing 8 family member C (LRRC8C) and TM4SF20 (Table 2). Inasmuch as TGF-β-induced cleavage of CREB3L1 is Smad4-independent (Figure 10B), we reasoned that Smad4 should also not be required for TGF-β to alter expression of genes encoding proteins regulating cleavage of CREB3L1. While knocking down Smad4 significantly inhibited activation of LRRC8C expression by TGF-β (Figure 11C), such treatment did not prevent TGF-β from inhibiting expression of TM4SF20 (Figure 11D). Similar to a slow but sustained induction of RIP of CREB3L1 by TGF-β, it took 24 h for TGF-β to suppress expression of TM4SF20 by more than 80%, and this suppression lasted for 3 days after the treatment with the cytokine (Figure 11E).

TM4SF20, a protein that has never been characterized before, belongs to a family of membrane proteins that contain four transmembrane domains (Wright et al., 2000). The results shown above suggest that TM4SF20 may act as an inhibitor for RIP of CREB3L1. If this is the case, then CREB3L1 is expected to be constitutively cleaved in cells in which expression of TM4SF20 is inhibited. To test this hypothesis, we transfected cells with two siRNA targeting different regions of TM4SF20. This treatment reduced the amount of the mRNA in cells that were not treated with TGF-β to the level similar to that in control siRNA-transfected cells treated with the cytokine (Figure 11F). Correlating with the reduction in TM4SF20 expression, CREB3L1 was cleaved even in the absence of TGF-β in cells transfected with the

siRNA targeting TM4SF20 (Figure 11G, lanes 3 and 5) but not those transfected with the control siRNA (Figure 11G, lane 1). This result suggests that TGF-β stimulates RIP of CREB3L1 through inhibition of *TM4SF20* expression. If this is the case, then overexpression of TM4SF20 should prevent TGF-β from inducing cleavage of CREB3L1. To test this hypothesis, a plasmid encoding myc epitope-tagged TM4SF20 was stably transfected into A549 cells to produce A549/pTM4SF20 cells. While TGF-β reduced expression of endogenous *TM4SF20* in parental A549 cells, it had no effect on expression of stably transfected *TM4SF20* in A549/pTM4SF20 cells (Figure 11H). Consequently, cleavage of CREB3L1 in these cells was not activated by TGF-β (Figure 11I).

TM4SF20 inhibits RIP of CREB3L1 by retaining the protein in the ER

Previous studies have demonstrated that Insig proteins, the inhibitors for RIP of SREBPs, block cleavage of SREBPs by retaining the proteins in the ER so that they are inaccessible to S1P and S2P, two Golgi-localized proteases catalyzing the RIP reaction (Yabe et al., 2002; Yang et al., 2002). We thus speculate that TM4SF20 may function through a similar mechanism by retaining CREB3L1 in the ER. If this is the case, then TM4SF20 should fulfill two requirements: The protein should be localized in the ER, and it should form a complex with the membrane-bound precursor of CREB3L1. To determine the subcellular localization of TM4SF20, we used anti-myc to detect localization of stably transfected TM4SF20 tagged with a myc epitope in A549/pTM4SF20 cells through immunofluorescent microscopy. The results showed that TM4SF20 displayed a typical ER staining pattern, and the protein co-localized with the ER marker calnexin (Figures 12A-D). TM4SF20 was not overexpressed overwhelmingly in A549/pTM4SF20 cells as the amount of TM4SF20 mRNA in the cells was only 4 fold higher than that in parental A549 cells (Figure 11H). Thus, the subcellular localization of the stably transfected TM4SF20 may be similar to that of the endogenous protein.

We performed a co-immunoprecipitation experiment to determine the interaction between TM4SF20 and CREB3L1 precursor. Nearly all membrane-bound CREB3L1 precursor was precipitated by anti-

CREB3L1 because the protein was depleted from the supernatant fraction of the immunoprecipitation carried out by anti-CREB3L1 but not a control antibody (Figure 12E, the 3rd panel). Again, we were unable to show the protein in the pellet fraction because of the interference of the heavy chain. TM4SF20 was only found in pellet fraction of immunoprecipitation carried out by anti-CREB3L1 but not the control antibody (Figure 12E, upper panel). This result suggests that TM4SF20 interacts with the CREB3L1 precursor.

TGF-β stimulates RIP of CREB3L1 through activation of ERKs

ERK activation has been implicated in pathological events of diseases caused by over-activation of the TGF-β-mediated signaling pathway (Holm et al., 2011). We thus investigated whether TGF-β inhibited expression of *TM4SF20* and stimulated the resultant RIP of CREB3L1 through ERK activation. Similar to CREB3L1 cleavage, TGF-β-induced activation of ERKs through phosphorylation was a slow but sustained response (Figure 13A). Treatment with RDEA119, a specific inhibitor of mitogen-activated protein kinase kinase (MEK) that phosphorylates and activates ERKs (Iverson et al., 2009), markedly inhibited TGF-β-induced phosphorylation of ERKs (Figure 13B). Correlating to the effect of RDEA119 on ERK phosphorylation, the compound significantly attenuated the inhibition of *TM4SF20* expression induced by TGF-β (Figure 13C). As a result, cleavage of CREB3L1 in cells treated with RDEA119 was no longer activated by TGF-β (Figure 13D).

3.5 Discussion

The results presented above support a model shown in Figure 14. In the absence of TGF-β, Smad2 and Smad3 remain inactive. These cells also synthesize TM4SF20 to retain CREB3L1 in the ER. As a result, CREB3L1 is not proteolytically activated as the protein is separated from the Golgi-localized proteases that catalyze the cleavage reaction. In the absence of activation of these transcription factors, transcription of genes involved in assembly of collagen extracellular matrix is not induced. Immediately after exposure of cells to TGF-β, Smad2 and Smad3 are activated by phosphorylation, and they form a complex with Smad4 to activate transcription of genes required for assembly of collagen matrix. TGF-β also activates ERKs through phosphorylation, resulting in inhibition of *TM4SF20* expression. Chronic exposure of the cells to TGF-β leads to deactivation of Smad2 and Smad3, as phosphorylation of these proteins is short-lived. In contrast to phosphorylation of the Smad proteins, phosphorylation of ERKs induced by TGF-β is a long-lasting event that leads to prolonged inhibition of *TM4SF20* expression. Owing to depletion of TM4SF20 in these cells, CREB3L1 is transported from the ER to Golgi where the protein is cleaved by S1P and S2P. This cleavage releases the NH_2-terminal domain of CREB3L1 from membranes, allowing it to form a complex with Smad4 to further activate transcription of genes required for synthesis of extracellular collagen matrix. Thus, proteolytic activation of CREB3L1 is crucial to activate genes involved in assembly of collagen matrix in cells chronically treated with TGF-β in which Smad2 and Smad3 are inactivated.

In contrast to the well-established canonical TGF-β signaling pathway mediated by Smad proteins, the functional significance of the Smad-independent non-canonical signaling pathway including ERK activation remains unclear(Massague, 2012). The ERK-mediated pathway was reported to contribute to aortic aneurysm progression in a mouse model of Marfan syndrome caused by excessive TGF-β signaling, but the underlying mechanism has not been identified (Habashi et al., 2011; Holm et al., 2011). In the current study we demonstrated that activation of ERKs was necessary for TGF-β to inhibit

expression of *TM4SF20,* a reaction required to activate RIP of CREB3L1. Interestingly, nuclear CREB3L1 produced through the RIP reaction requires Smad4 as a co-activator to simulate transcription of genes involved in assembly of collagen extracellular matrix. Thus, the canonical and the non-canonical signaling pathway of TGF-β are both required to induce collagen synthesis, and the two pathways are connected during the signaling event.

The current study expands our knowledge toward RIP by identifying TM4SF20 as an inhibitor for RIP of CREB3L1. We show that TM4SF20 is localized in the ER and forms a complex with membrane-bound precursor of CREB3L1. These results suggest that TM4SF20 may inhibit RIP of CREB3L1 by retaining CREB3L1 in the ER. This mechanism is similar to that used by Insig-1, another ER membrane protein that is the predominant Insig isoform expressed in cultured cells (Sever et al., 2004), to inhibit RIP of SREBPs in these cells. SREBPs form a complex with Scap, a membrane-bound cholesterol sensor (Radhakrishnan et al., 2004; Sakai et al., 1997). In cells loaded with cholesterol and unsaturated fatty acids, Insig-1 binds to Scap, a reaction retaining the Scap/SREBPs complex in the ER thereby preventing RIP of SREBPs (Yang et al., 2002). Deprivation of cholesterol or unsaturated fatty acids stimulates proteasomal degradation of Insig-1 (Gong et al., 2006; Lee et al., 2006; Lee et al., 2008). Consequently, Scap escorts SREBPs from the ER to Golgi where SREBPs are cleaved by S1P and S2P (Brown and Goldstein, 2009). Thus, TGF-β-induced RIP of CREB3L1 is mechanistically similar to lipid deprivation-induced RIP of SREBPs as both processes reduce the amount of proteins that inhibit the RIP reactions.

It was reported previously that bone morphogenetic protein 2 (BMP2) stimulates RIP of CREB3L1 to produce collagen in osteoblasts (Murakami et al., 2009). Although BMP2 and TGF-β belong to the same family of cytokines that signal through the Smad proteins (Massague, 2012), BMP2 uses a different mechanism to stimulate RIP of CREB3L1: Unlike TGF-β, BMP2 appears to induce cleavage of CREB3L1 through ER stress (Murakami et al., 2009). BMP2 also takes much longer time (~7 days) to

induce cleavage of CREB3L1 than that required for TGF-β to induce the same reaction (Murakami et al., 2009). Future studies are required to determine the mechanism through which BMP2 induces proteolytic activation of CREB3L1.

In addition to inducing genes involved in assembly of collagen matrix, nuclear CREB3L1 also activates genes that suppress cell proliferation (Denard et al., 2012; Denard et al., 2011). Interestingly, TGF-β was originally discovered as a cytokine that inhibited proliferation of certain cells (Massague, 2008). Thus, RIP of CREB3L1 may also be involved in TGF-β-mediated suppression of cell proliferation. However, this function of TGF-β is frequently inactivated in malignant tumor cells\(Massague, 2008, 2012), including A549 cells that were used in the current study (data not shown). If RIP of CREB3L1 is indeed required for TGF-β to suppress cell proliferation, then these tumor cells may prevent nuclear CREB3L1 from activating genes involved in suppression of cell cycle. Compared to complete inactivation of RIP of CREB3L1, this strategy may provide more benefit for cancer cells as it still allows production of collagen extracellular matrix, which has been reported to facilitate metastasis of the tumor cells (Cheng and Leung, 2011; Li et al., 2010; Shintani et al., 2008a; Shintani et al., 2008b). A possible mechanism through which cancer cells specifically prevents nuclear CREB3L1 from activating transcription of genes encoding proteins that inhibit cell proliferation is to inactivate the transcriptional co-activator that is required to induce these genes. Our current and previous studies (Denard et al., 2011) demonstrate that nuclear CREB3L1 is required but not sufficient to induce its target genes. In the current study we identify Smad4 as a co-activator that is required for nuclear CREB3L1 to induce genes involved in assembly of collagen extracellular matrix. Identification of the co-activator required for nuclear CREB3L1 to stimulate genes involved in suppression of cell proliferation may reveal the mechanism through which cancer cells escape TGF-β-induced cytostatic effect.

The current study demonstrates that RIP of CREB3L1 is not required for TGF-β to activate most genes involved in EMT except for those required for assembly of collagen matrix. The pathway is even

not required for TGF-β to acutely induce transcription of *COL1A1*. The specific requirement of this pathway for TGF-β to chronically induce transcription of genes involved in assembly of collagen extracellular matrix makes RIP of CREB3L1 a possible drug target to treat fibrotic disease, which is caused by chronic deposition of excess collagen matrix on tissue surface (Rosenbloom et al., 2010). RIP of CREB3L1 can be blocked through inhibition of S1P (Denard et al., 2012; Denard et al., 2011). S1P inhibitors have been developed mainly for inhibiting lipid synthesis by blocking RIP of SREBPs (Hawkins et al., 2008; Olmstead et al., 2012). We also demonstrated that RDEA119, a MEK inhibitor originally designed for cancer treatment (Iverson et al., 2009), was effective in blocking RIP of CREB3L1. It will be interesting to determine the effect of these compounds on treating fibrotic diseases.

3.6 Chapter Tree Figures

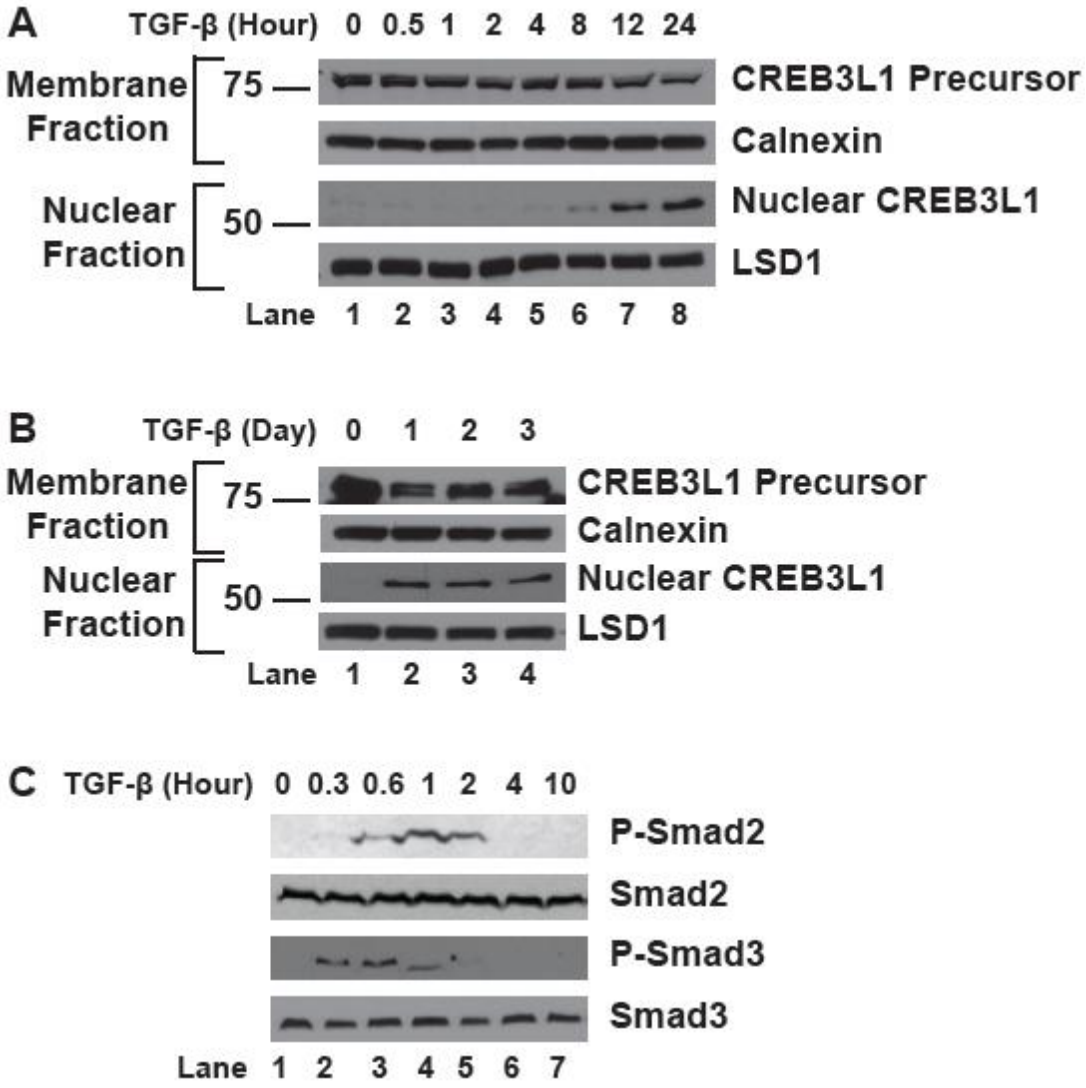

Figure 8. TGF-β induces RIP of CREB3L1.
(A - C) On day 0, A549 cells were seeded at 4×10^5 cells per 60-mm dish. On day 1, cells were treated with 1 ng/ml TGF-β for the indicated time. For treatment longer than 24 h, cells were changed to fresh medium containing TGF-β once every 24 h. (A and B) Cells were then harvested and separated into nuclear and membrane fractions, and analyzed by immunoblot analysis with indicated antibodies. Immunoblot analysis with antibodies against calnexin and lysine-specific demethylase 1 (LSD1) served as loading control for membrane and nuclear fractions, respectively. (C) Cells were harvested and cell lysates were analyzed through immunoblot analysis with indicated antibodies.

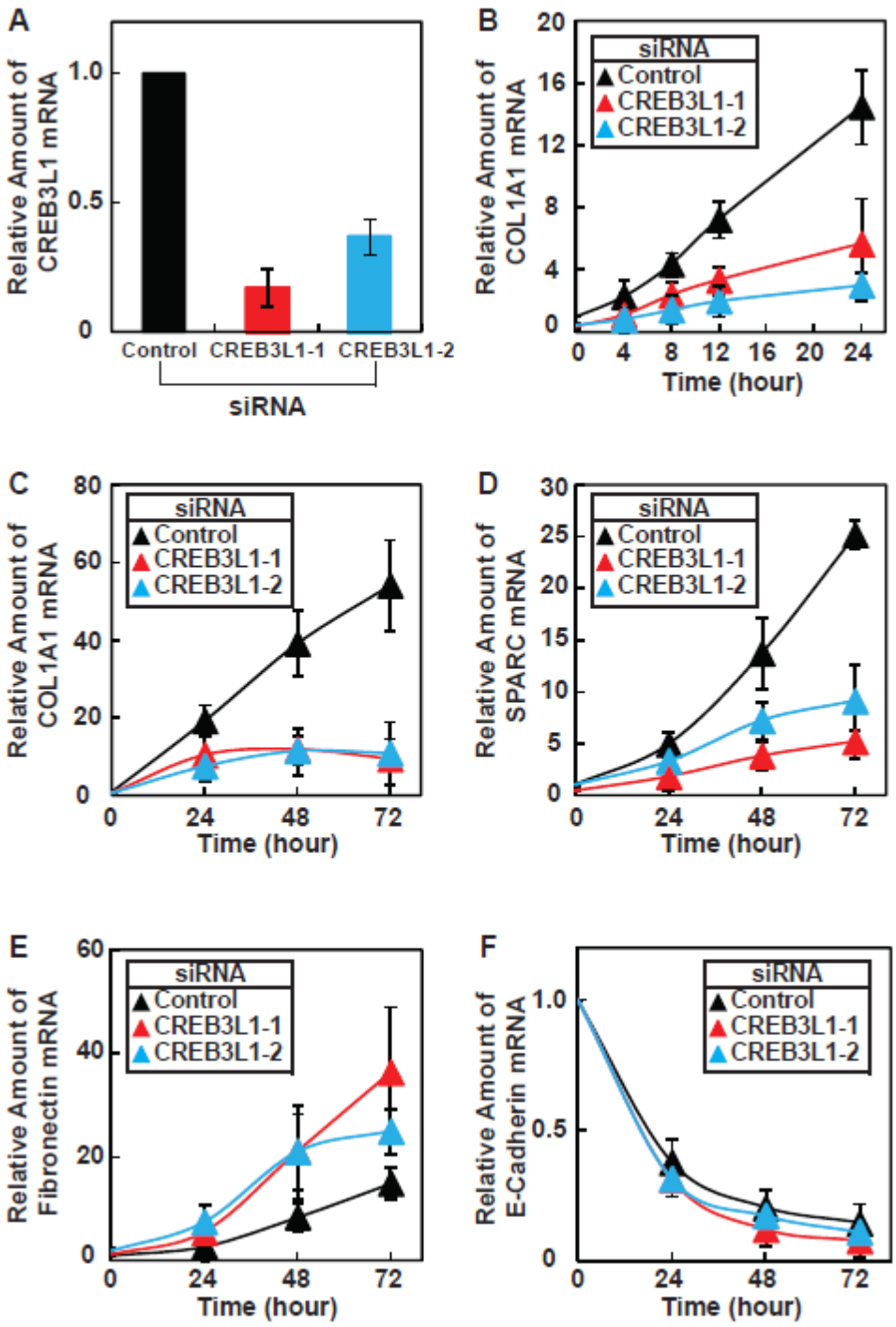

Figure 9. Sustained induction of collagen synthesis by TGF-β requires CREB3L1.
(A-F) On day 0, A549 cells were seeded at 1 × 10^5 cells per 60 mm dish. On day 1, the cells were transfected with indicted siRNAs. (A) On day 3, cells were harvested for quantification of CREB3L1 mRNA by real time-quantitative PCR (RT-QPCR). The amount of the mRNA in cells transfected with the control siRNA is set to 1. (B-F) On day 3, cells were treated with 0.5 ng/ml TGF-β for the indicated time as described in Figure 1. Cells were then harvested for quantification of indicated mRNA through RT-QPCR. The amount of the indicated mRNA in cells transfected with the control siRNA immediately

before the TGF-β treatment is set to 1. (A-F) Results are reported as mean ± S.E.M. of three independent experiments.

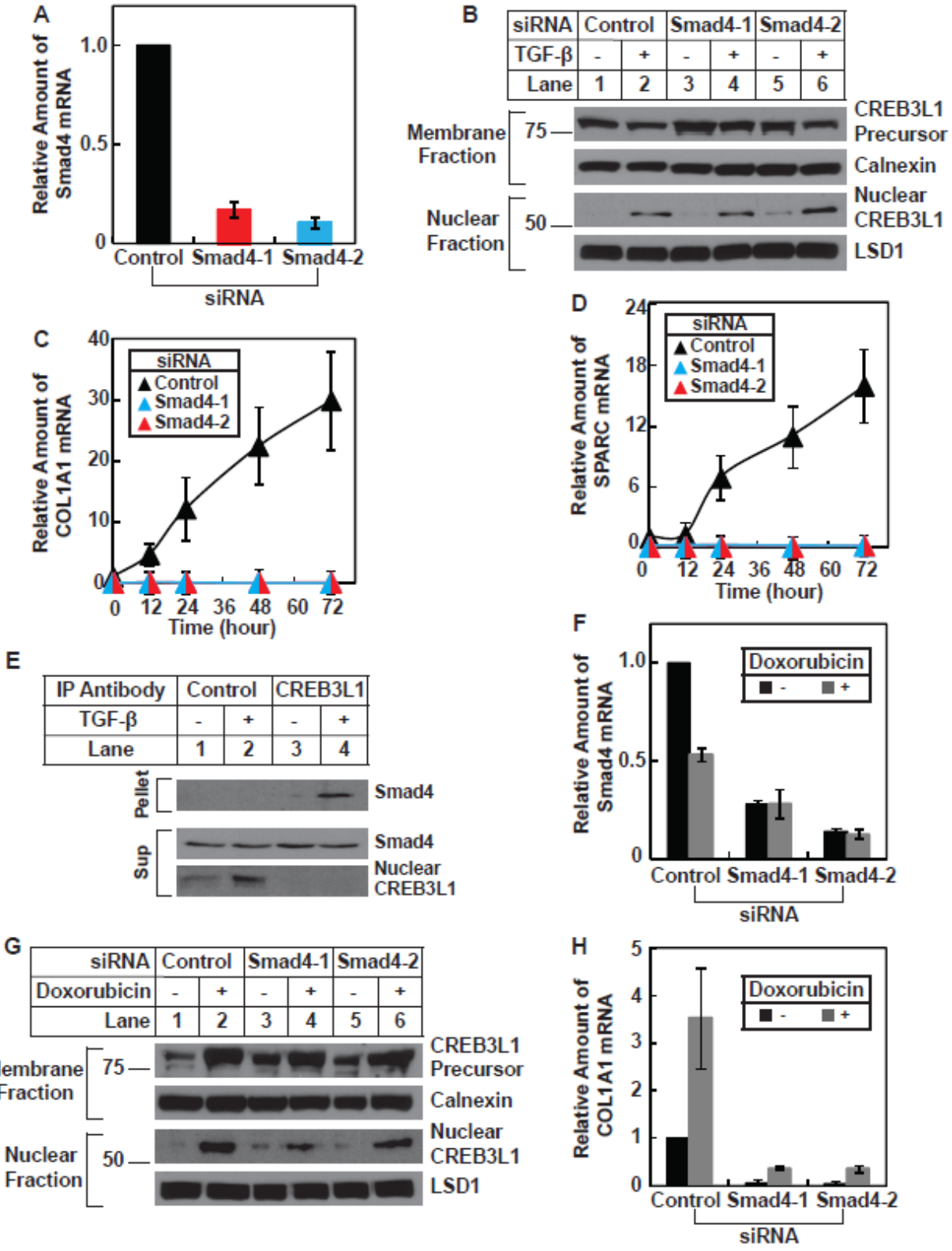

Figure 10. SMAD4 is a co-factor for CREB3L1 to induce transcription of *COL1A1* and *SPARC*.

(A) Quantification of Smad4 mRNA through RT-QPCR following transfection of indicated siRNA was performed as described in Figure 2A.
(B) On day 0, A549 cells were seeded at 1×10^5 cells per 60 mm dish. On day 1, the cells were transfected with indicted siRNAs. On day 3, cells were treated with or without 1 ng/ml TGF-β. On day 4, 24 hr after the treatment, cells were harvested and analyzed as in Figure 1A.
(C-D) Quantification of the indicated mRNA following transfection with the indicated siRNA and treatment with TGF-β for the indicated time was performed as described in Figure 2B.
(E) On day 0, A549 cells were seeded at 4×10^5 cells per 60 mm dish. On day 1, cells were treated with or without 1 ng/ml TGF-β. On day 2, 24 hr after the treatment, cells were harvested. Cell lysates were subjected to immunoprecipitation with the indicated antibodies. The immunoprecipitates (pellet) from 2 dishes of the cells and supernatant (sup) from 0.7 dishes of the cells were analyzed by immunoblot analysis with the indicated antibodies.
(F-H) On day 0, Huh7 cells were seeded at 5×10^4 cells per 60 mm dish. On day 1, cells were transfected with indicted siRNAs. On day 3, cells were treated with or without 500 nM doxorubicin. (F and H) On day 4, 24 h after the treatment, cells were harvested for quantification of indicated mRNA by RT-QPCR. The amount of the mRNA in cells that were not treated with doxorubicin and transfected with the control siRNA is set to 1. (G) On day 4, 24 h after the treatment, cells were harvested and RIP of CREB3L1 was analyzed as described in Figure 2A.
(A, C, D, F and H) Results are reported as mean ± S.E.M. of three independent experiments.

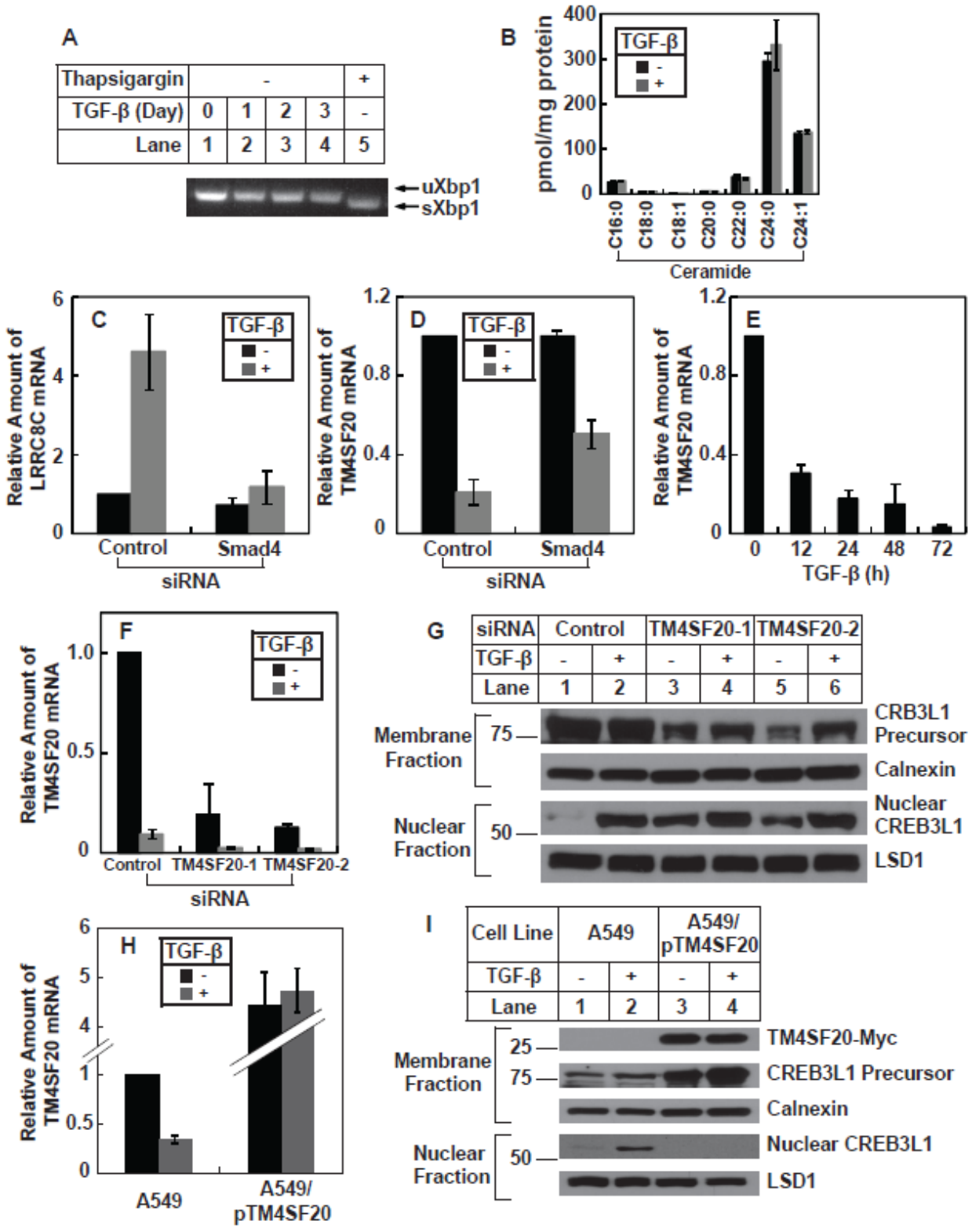

Figure 11. TGF-β induces CREB3L1 cleavage by inhibiting expression of *TM4SF20*.
(A) A549 cells treated with 1 ng/ml TGF-β for the indicated time or 1 μM thapsigargin (as a positive control to stimulate ER stress) for 4 h were harvested for analysis of Xbp1 splicing through RT-PCR as

described in Supplementary Experimental Procedure. U and S denote unspliced and spliced Xbp1, respectively.

(B) A549 cells treated with or without 3 ng/ml TGF-β for 24 h were harvested for ceramide analysis as described in Supplementary Experimental Procedure. The amount of ceramide with indicated amide-linked fatty acids was presented.

(C-D) On day 0, A549 cells were seeded at 1×10^5 cells per 60 mm dish. On day 1, the cells were transfected with indicted siRNAs. On day 3, cells were treated with or without 1 ng/ml TGF-β for 12 h. cells were then harvested for quantification of indicated mRNA by RT-QPCR. The amount of the mRNA in cells that were not treated with TGF-β and transfected with the control siRNA is set to 1.

(E) On day 0, A549 cells were seeded at 4×10^5 cells per 60 mm dish. On day 1, the cells were treated with 1 ng/ml TGF-β for the indicated time. Cells were then harvested for quantification of TM4SF20 mRNA by RT-QPCR. The amount of the mRNA in cells immediately before the TGF-β treatment is set to 1.

(F and G) On day 0, A549 cells were seeded at 1×10^5 cells per 60 mm dish. On day 1, the cells were transfected with indicted siRNAs. On day 3, cells were treated with or without 1 ng/ml TGF-β. On day 4, 24 h after the treatment, cells were harvested for quantification of TM4SF20 mRNA as described in A (D), and analysis of RIP of CREB3L1 as described in Figure 1A (E).

(H and I) On day 0, A549 and A549/pTM4SF20 cells were seeded at 4×10^5 cells per 60 mm dish. On day 1, cells were treated with or without 1 ng/ml TGF-β. On day 2, 24 h after the treatment, cells were harvested for quantification of TM4SF20 mRNA by RT-QPCR, with the amount of the mRNA in A549 cells that were not treated with TGF-β set to 1 (F), and analysis of RIP of CREB3L1 as described in Figure 1A (G).

(A-G) Bar graphs are reported as mean ± S.E.M. of three independent experiments.

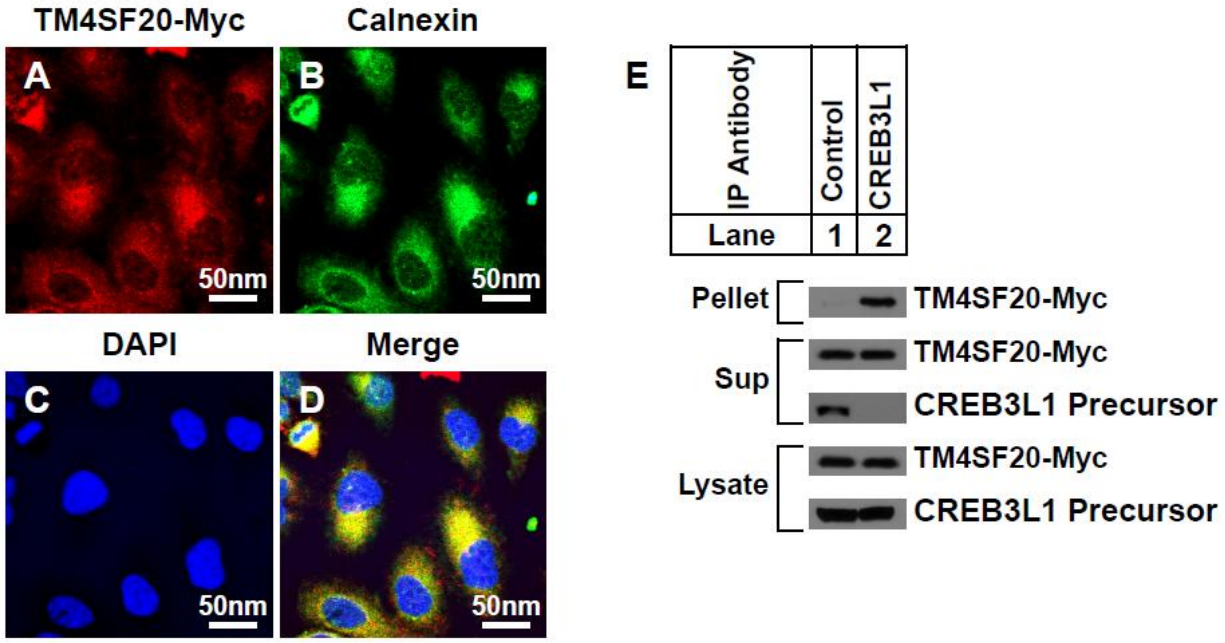

Figure 12. TM4SF20 retains CREB3L1 in the ER.
(A-D) On day 0, A549/pTM4SF20 cells were seeded at 2×10^5 per well on a cover slip placed in a 6-well plate. On day 1, the cells were fixed and analyzed by immunofluorescent microscopy as described in Experimental Procedures. Representative images stained by anti-Myc to detect stably transfected TM4SF20 (A), by anti-calnexin to detect the ER marker calnexin(B), by DAPI to detect cell nucleus (C), and the merged images (D) were shown.
(E) On day 0, A549/pTM4SF20 cells were seeded at 4×10^5 cells per 60 mm dish. On day 1, cells were harvested, and cell lysates were subjected to immunoprecipitation with the indicated antibody. The cell lysates (from 0.35 dishes of cells), immunoprecipitates (pellet, from 2.5 dishes of cells) and supernatant (sup, from 0.7 dishes of cells) were analyzed by immunoblot analysis with anti-CREB3L1 or anti-Myc to detect stably transfected CREB3L1.

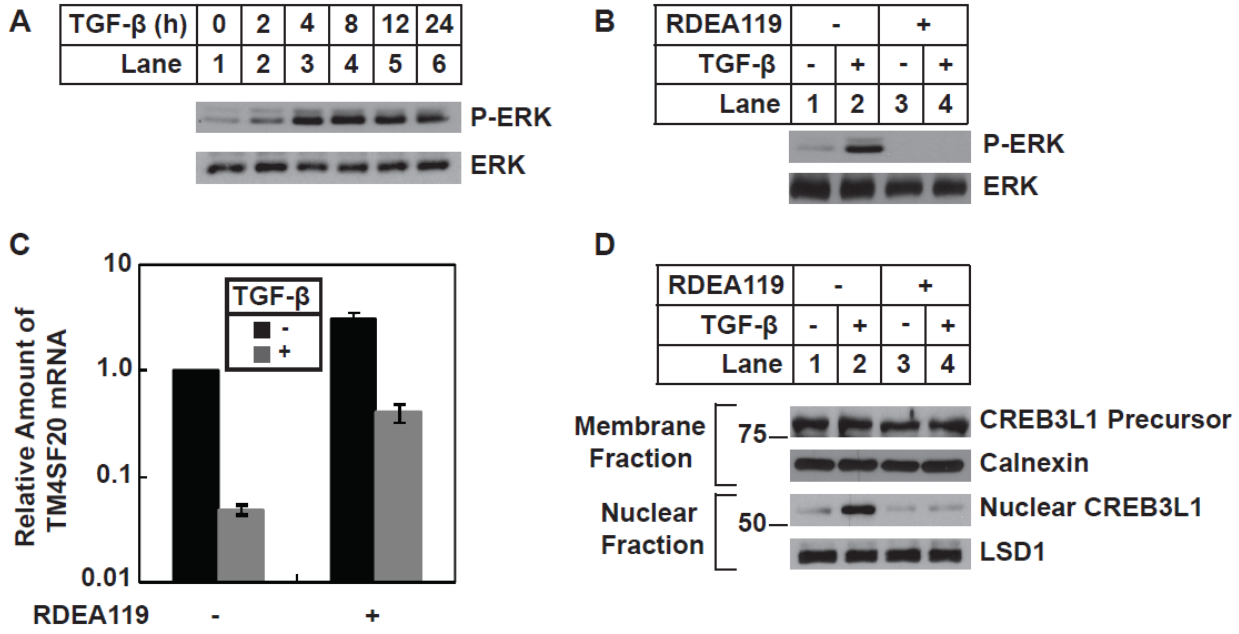

Figure 13. TGF-β induces cleavage of CREB3L1 through activation of ERKs

(A) A549 cells were set up and treated as described in Figure 1C and analyzed with immunoblot with indicated antibodies.

(B-D) On day 0, A549 cells were seeded at 4×10^5 cells per 60 mm dish. On day 1, cells were treated with 0.5 μM RDEA119 for 3 h followed by treatment with 1 ng/ml TGF-β as indicated. On day 2, 24 h after the TGF-β treatment, cells were harvested for immunoblot analysis with indicated antibodies (B and D) and quantification of TM4SF20 mRNA with RT-QPCR, with the amount of the mRNA in cells treated with neither RDEA119 nor TGF-β set to 1α (C).

(C) Results are reported as mean ± S.E.M. of three independent experiments.

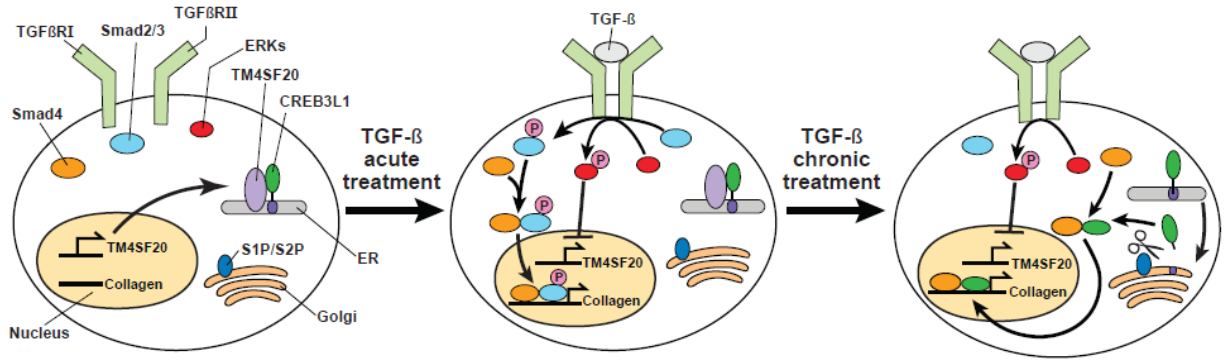

Figure 14. A model illustrating the role of CREB3L1 in TGF-β-induced collagen synthesis
In the absence of TGF-β, Smad2 and Smad3 (Smad2/3) are not phosphorylated. TM4SF20 is expressed at an amount sufficient to block RIP of CREB3L1 by retaining CREB3L1 precursor in the ER. In the absence of activation of these transcription factors, expression of *collagen* is not induced. Acute exposure of cells to TGF-β results in heterodimerization of two TGF-β receptors, namely TGFβRI and TGFβRII. Consequently, Smad2/3 are phosphorylated by the activated receptor, allowing them to form a complex with Smad4 to drive transcription of *collagen*. TGF-β treatment also leads to phosphorylation of ERKs, which in turn inhibit transcription of *TM4SF20*. In cells chronically exposed to TGF-β, the amount of phosphorylated Smad2/3 is drastically reduced. Owing to depletion of TM4SF20, CREB3L1 precursor is transported from the ER to Golgi where it is cleaved by S1P and S2P. This cleavage releases the NH_2-terminal domain of CREB3L1 from membranes, allowing it to form a complex with Smad4 to activate transcription of *collagen*.

CHAPTER FOUR:

Ceramide Regulates RIP of CREB3L1 through Alternative Translocation of TM4SF20

4.1 Abstract

Ceramide stimulates proteolytic cleavage of CREB3L1, yet the mechanism through which it activates CREB3L1 is not clear. Here we reported that ceramide induced alternative translocation of TM4SF20: In the absence of ceramide, the NH_2-terminus of TM4SF20 was used as a signal sequence to insert the polytopic membrane protein in the ER and was removed from mature protein through cleavage catalyzed by signal peptidase. Upon treatment with ceramide, the NH_2-terminus of TM4SF20 was no longer recognized as signal sequence. Instead, the NH_2-terminus of newly synthesized TM4SF20 proteins were located in the cytosol, resulting in alternative translocation of the protein that adopted an opposite membrane topology. We further demonstrated that insertion of the signal sequence of TM4SF20 into ER in the absence of ceramide required translocation associated membrane protein 2 (TRAM2), as knockdown of TRAM2 led to alternative translocation of TM4SF20 even in the absence of the lipid. Since TRAM2 contains a domain known to bind ceramide, we suspect that ceramide inhibits the function of TRAM2 so that alternative translocation of TM4SF20 occurs. These results suggest that ceramide may induce RIP of CREB3L1 by inactivating TM4SF20 through alternative translocation.

4.2 Introduction

Ceramide is a sphingolipid whose formation is induced by exposure to chemotherapy. Recently, it is found that doxorubicin, a chemotherapy drug, increases the amount of ceramide by inducing the *de novo* synthesis pathway (Denard et al., 2012). The accumulation of ceramide is required for doxorubicin to stimulate proteolytic cleavage of CREB3L1. Activation of CREB3L1 induces transcription of genes encoding inhibitors of the cell cycle (Denard et al., 2012). Although it is predicted that ceramide induces RIP of CREB3L1 by triggering the transport of CREB3L1 from ER to Golgi, the underlying mechanism remains unclear.

TM4SF20 is a membrane protein preventing RIP of CREB3L1 by retaining CREB3L1 in the ER. TGF-β stimulates RIP of CREB3L1 by inhibiting expression of the protein. However, the role of TM4SF20 in RIP of CREB3L1 induced by ceramide has not been examined. Since TM4SF20 is a transmembrane protein, it needs to be inserted in the ER membrane. One paradigm for membrane protein insertion is the signal sequence pathway. Signal sequence is located at the NH_2-terminus of proteins and usually contains a stretch of hydrophobic amino acids. It is thought that membrane protein is co-translationally translocated into ER membrane (Shao and Hegde, 2011). During translational translocation, the signal sequence within a nascent polypeptide is recognized by signal recognition particle (SRP), targeted to the ER membrane via SRP receptor (SR), and transferred to the Sec61 translocation channel (Shao and Hegde, 2011). Of the various translocation components, translocating-chain associating membrane (TRAM) proteins could play a role in stimulating the translocation of proteins with weak signal sequences that are less hydrophobic.(Shao and Hegde, 2011; Voigt et al., 1996). Mammalian cells express three TRAM proteins: TRAM1, TRAM2 and TRAM1L1. Sequence alignment showed that TRAM proteins share a TRAM-Lag1p-CLN8 (TLC) domain with ceramide synthase (Winter and Ponting, 2002). However, the effect of ceramide on TRAM proteins has never been determined.

In the current study, we demonstrate that in the absence of ceramide, the NH_2-terminus of TM4SF20 was used as signal sequence in a TRAM2-dependent manner. Upon treatment with ceramide, the NH_2-terminus of TM4SF20 was no longer recognized as signal sequence, presumably because the function of TRAM2 was inhibited by ceramide. As a result, ceramide triggered alternative translocation of TM4SF20 to produce a protein adopting a membrane topology opposite to that of the protein in the absence of the lipid. We speculate that ceramide-induced alternative translocation of TM4SF20 may inactivate the protein to stimulate RIP of CREB3L1.

4.3 Material and Methods

Materials

We obtained rabbit anti-actin from Sigma (St. Louis, MO); mouse anti-HSV from Novagen (Madison, WI); peroxidase-conjugated secondary antibodies from Jackson ImmunoResearch (West Grove, PA). Hybridoma cells producing IgG-9E10, a mouse monoclonal antibody against Myc tag, were obtained from the American Type Culture Collection (Manassas, VA).

Plasmid

pCMV-TM4SF20-$(Myc)_5$ encodes full length human TM4SF20 followed by 5 tandem repeats of the myc epitope tag. It is produced by ligating BamHI and NheI-cleaved vector pcDNA3.1-$(Myc)_5$ (Wang et al., 2005) with the PCR product corresponding to full length TM4SF20.

pCMV-$(Myc)_5$-TM4SF20 encodes full length human TM4SF20 with 5 tandem repeats of the myc epitope tagged to NH_2-terminus. It is produced by ligating AgeI-cleaved vector pcDNA3.1-$(Myc)_5$ (Wang et al., 2005) with the PCR product corresponding to full length TM4SF20.

pCMV-TM4SF20(1-36)-PLAP(18-507)-$(Myc)_5$ encodes an COOH-terminal tagged fusion protein consisting of amino acids 1 to 36 of TM4SF20, two amino acids (AS) encoded by the sequence for restriction site NheI, amino acids 18 to 507 of human placental alkaline phosphotase, and five tandem copies of the myc epitope. Intermediate construct pCMV-TM4SF20(1-36)-$(Myc)_5$ was obtained using the same strategy as making pCMV-TM4SF20-$(Myc)_5$ except PCR product corresponding to amino acids 1-36 of TM4SF20. The nucleotide sequence encoding amino acids 18-507 of PLAP was obtained from a previously described construct pCMV-PLAP-BP2 (513-1141) (Sakai et al., 1998). The amplified product was digested with NheI and cloned into the unique site NheI site between TM4SF20(1-36) and the five tandem myc epitope.

All constructs in which the expressions were driven by thymidine kinase promoter were obtained by polymerase chain reaction on constructs in which the expressions were driven by CMV promoter with primers containing HindIII and XbaI sites. HindII restriction site was inserted into a previously described construct pTK-HSV-CREB3L1(Denard et al., 2011) after NheI restriction site through site-directed mutagenesis. The amplified product was digested with HindIII and XbaI and cloned into the pre-digested vector.

Site-directed mutagenesis

Oligonucleotide site-directed mutagenesis was carried out with complementary primers using QuickChange Site-Directed Mutagenesis kit from stratagene (La Jolla, CA). The mutations were confirmed by sequencing the relevant region.

Cell culture

A549 cells were maintained in medium A (1:1 mixture of Ham's F12 medium and Dulbecco's modified Eagle's medium containing 100 U/ml penicillin and 100 µg/ml streptomycin sulfate supplemented with 5% [vol/vol] fetal calf serum (FCS). A549/pTM4SF20 cells were generated by transfecting pCMV-TM4SF20-$(Myc)_5$ followed by selection with 700 µg/ml G418. The cells were maintained in medium A supplemented with 700 µg/ml G418. Cells were cultured in monolayers at 37°C in 8.8% CO_2.

Immunoblot analyses

Cells were harvested and separated into nuclear and membrane fractions as described (Sakai et al., 1996), and analyzed by SDS-PAGE followed by immunoblot analysis with the indicated antibodies (1:2000 dilution for anti-Myc, anti-actin). Bound antibodies were visualized with a peroxidase-conjugated secondary antibody using the SuperSignal ECL-HRP substrate system (Pierce).

RNA interference

Duplexes of siRNA were synthesized by Dharmacon Research. The two siRNA sequences targeting human TRAM1 are GAUAAUUAUUCAUGCCGUA and CCGUAAUUCAAGAGUAUAU. The two siRNA sequences targeting human TRAM2 are UGGAAUGAGCAGAGUGCAA and GGCAUUUGAUCCCGAGAAA. The control siRNA targeting GFP was reported previously (Adams et al., 2004). Cells were transfected with siRNA using Lipofectamine RNAiMAX reagent (Invitrogen) as described by the manufacturer, after which the cells were used for experiments as described in the figure legends.

RT-QPCR

RT-QPCR was performed as previously described (Liang et al., 2002). Each measurement was made in triplicate from cell extracts pooled from duplicate dishes. The relative amounts of RNAs were calculated through the comparative cycle threshold method by using human 36B4 mRNA as the invariant control.

Vesicle preparation

Intact membrane vesicles were prepared as described before (Feramisco et al., 2004). Briefly, cell pellets from triplicate dishes were resuspended in 0.4 ml of Buffer A1 (10mM Hepes-KOH (pH 7.4), 10mM KCl, 1.5mM $MgCl_2$,5mM sodium EDTA, 5mM sodium EGTA, and 250mM sucrose), passed through a 22.5-gauge needle 20 times, and centrifuged at 1000×g for 5min at 4˚C. The supernatant was subjected to centrifugation at 2×10^4 ×g for 30 min at 4˚C. The resulting pellets were resuspended in buffer A2 (Buffer A1 containing 100mM NaCl).

Protease K treatment

Protease K treatment was performed as described before with minor modifications (Feramisco et al., 2004): Aliquots of membranes (50μg of proteins) were treated with indicated amount of protease K in the absence or presence of 1% NP-40 in a total volume of 50μl buffer A2 for 1h at 37˚C. After incubation,

12.5µl of laemmli buffer (150mM Tris-HCl (pH 6.8), 15% SDS, 25% glycerol, 0.02% (w/v) bromophenol blue, 12.5% (v/v) 2-mercaptoethanol) was added and samples were boiled for 5min. All the samples were subjected to SDS/PAGE and immunoblot analysis.

4.4 Results

Ceramide induces glycosylation of TM4SF20

To analyze proteolytic activation of CREB3L1, we transfected A549 cells with a plasmid pTK-HSV-CREB3L1 encoding full length CREB3L1 preceded with two copies of the HSV epitope tag (QPELAPEDPED) at the NH_2-terminus, fractionated A549 cells into membrane and nuclear fractions and used an antibody reacting against HSV tag to examine the cleavage of CREB3L1 through immunoblot analysis. In the absence of treatment, CREB3L1 existed as the full length precursor (~80 kDa) (Figure 15A, lane 1, middle panel) and the nuclear CREB3L1 (~55kDa) was undetectable (Figure 15A, lane1, upper panel). When cells were treated with either TGF-β or ceramide, the amounts of nuclear CREB3L1 were increased (Figure 15A, lane 2 and 3, upper panel). This was consistent with previously reported results: TGF-β and ceramide stimulated proteolysis of CREB3L1 (Denard et al., 2012).To determine whether TM4SF20 blocks RIP of CREB3L1 induced by TGF-β and ceramide, a plasmid pCMV-TM4SF20-$(Myc)_5$ encoding full length TM4SF20 with five copies of the myc epitope tag at the COOH-terminus was co-transfected with HSV epitope-tagged CREB3L1 into A549 cells. Expression of TM4SF20 blocked the cleavage of CREB3L1 induced by TGF-β (Figure 15A, lane 2 and 5, upper panel). Surprisingly, overexpression of TM4SF20 had no effect on ceramide-induced cleavage of CREB3L1 (Figure 15A, lane 3 and 6, upper panel). This result suggests that ceramide induces RIP of CREB3L1 through a mechanism that is different from that employed by TGF-β. We then determined the expression of TM4SF20. To our surprise, besides the band with expected molecular weight (~23 kDa) (Figure 15A, lane 4 to 6, lower panel), ceramide induced another form of TM4SF20 that migrated much slower in SDS/PAGE (~45 kDa) (Figure 15A, lane 6, lower panel).

We then determined the modification that resulted in the appearance of the higher form of TM4SF20. Hydrophobicity plot analysis showed that TM4SF20 has four putative transmembrane domains, and there are three potential glycosylation sites in the loop between the third and forth

transmembrane domains (Figure 15B). To determine if the higher form of TM4SF20 was glycosylated, we treated lysate from ceramide-treated cells with either EndoH or PNGase F, two enzymes that are known to remove N-linked carbohydrates. Treatment with EndoH or PNGase F increased the mobility of the higher form of TM4SF20 induced by ceramide (Figure 15C), suggesting that this form of TM4SF20 was glycosylated. However, the band did not shift to the same position as the lower form (Figure 15C), suggesting that there was other modification besides N-linked glycosylation. Because PNGase F only cleaved the linkage between asparagine and N-acetylglucosamines, we speculated that the higher form of TM4SF20 may also have O-linked glycosylation.

To further demonstrate that the higher form of TM4SF20 was glycosylated, we transfected A549 cells with plasmids encoding either wild-type TM4SF20 (Figure 15D, lane 1 and 2) or mutants with each of the potential glycosylation sites mutated to glutamine (N132Q, N148, and N163Q) (Figure 15D, lane3-8). Mutation disrupting each glycosylation reduced the molecular weight of the higher form (Figure 15D, asterisk indicates a non-specific band), an observation suggesting that each of the three sites was glycosylated. To determine if only these three sites were glycosylated, we transfected A549 cells with plasmids encoding either wild-type TM4SF20 (Figure 15E, lane 1and 2) or a mutant with all three glycosylation sites disrupted (N132Q/N148Q/N163Q) (Figure 15E, lane 3 and 4). This mutant showed resistance to PNGase F treatment and had the same mobility as PNGase F-treated wild-type proteins (Figure 15E). These results suggest that the higher form of TM4SF20 induced by ceramide was glycosylated and only glycosylated at position 132, 148 and 163.

Ceramide induces alternative translocation of TM4SF20

Because glycosylation reactions occur in the lumen of the ER, the unglycosylated and glycosylated form of TM4SF20 may have different orientation in ER membrane. To determine the membrane topology of TM4SF20 in the ER, we then tried to localize the COOH-terminus of TM4SF20 with respect to the ER membrane using protease K protection assay. We used A549/pTM4SF20 cells in which a plasmid

encoding full length TM4SF20 with five myc epitope tagged to COOH-terminus was stably transfected into A549 cells. A549/pTM4SF20 cells were left untreated or treated with ceramide. Intact ER membrane vesicles were isolated, and treated with protease K in the absence or presence of NP-40. The samples were then subjected to SDS/PAGE followed by immunoblotting with an antibody against the myc tag. In the absence of protease K, only the unglycosylated form of TM4SF20 can be detected (Figure 16A, lane 1). TM4SF20 from ceramide-treated cells appeared as both the glycosylated form and the unglycosylated form (Figure 16A, lane 13). Small amount of protease K destroyed the epitope of the glycosylated form of TM4SF20 (Figure 16A, lane 13-18). The results were similar in the presence of NP-40 (Figure 16A, lane 19-24). On the contrary, in the absence of NP-40, the epitope of the unglycosylated form of TM4SF20, remained intact until extreme high levels of protease K were used (Figure 16A, lane 1-6). In the presence of NP-40, the epitope of the lower band was also quickly destroyed by small amount of protease K (Figure 16A, lane 7-12). These results suggested that the COOH-terminus of the unglycosylated form of TM4SF20 was protected in the ER lumen. On the contrary, the COOH-terminus of the glycosylated form of TM4SF20 was located in the cytosol.

To determine the membrane orientation of NH_2-terminus of TM4SF20, we transfected cells with a plasmid encoding full length TM4SF20 with five copies of the myc epitope tag at the NH_2-terminus. Surprisingly, although we detected ceramide-induced glycosylated form of TM4SF20 when myc epitope was tagged to NH_2-terminus of TM4SF20, the unglycosylated form of TM4SF20 was undetectable either in the absence or presence of ceramide (Figure 16B, lane2-3). This result led us to speculate that in the absence of ceramide, the NH_2-terminus of TM4SF20 was used as signal sequence and removed from the mature protein by cleavage of signal peptidase. Then we performed protease K protection assay and the result suggested that in the presence of ceramide, the NH_2-terminus of glycosylated form of TM4SF20 also faced the cytosol (Figure 16C).

The results shown above suggest that TM4SF20 may exist as two forms with different membrane topology. In the absence of ceramide, the NH_2-terminus of TM4SF20 is used as signal sequence which is cleaved off from the mature protein by signal peptidase. As a result, the COOH terminus of TM4SF20 is located in the ER lumen and the hydrophilic loop between third and fourth transmembrane is located in the cytosol preventing glycosylation of this protein (Figure 16D, left panel). Upon treatment with ceramide, the NH_2-terminus is no longer recognized as a signal sequence. Consequently, the NH_2- and COOH-terminus are both located in the cytosol and the glycosylation sites are located in the ER lumen, allowing modification of TM4SF20 (Figure 16D, right panel). This phenomenon was designated as alternative translocation (Figure 16D).

Since membrane proteins are inserted in ER membrane during translation, the glycosylated form of TM4SF20 induced by ceramide is likely to be newly synthesized proteins. To test this hypothesis, we treated cells with cycloheximide, an inhibitor for protein synthesis. This treatment inhibited ceramide-induce the glycosylated form of TM4SF20 (Figure 16E), suggesting that the glycosylated form of TM4SF20 induced by ceramide was indeed newly translated protein.

First transmembrane of TM4SF20 is important for alternative translocation

To determine the amino acid residues that are important for alternative translocation of TM4SF20, we made a systematic series of mutations in the predicted signal peptide, but were unable to identify any mutations that disrupt ceramide-induced alternative translocation of TM4SF20. We then focused on the first transmembrane domain (L15 to V35) that is immediately following the signal sequence. Helical wheel analysis indicated that this transmembane helix contained a surface that is less hydrophobic composed by G22 and N26 (Figure 17A). To test the importance of this surface on alternative translocation of TM4SF20, we mutated these residues to leucine. When TM4SF20 had a mutation of G22L (Figure 17B) or N26L (Figure 17C), it constitutively went through alternative translocation and

was glycosylated even without ceramide treatment. This result indicates glycine 22 and asparagine 26 are important for signal sequence recognition.

TRAM2 is required for signal sequence recognition of TM4SF20

We then determined the mechanism through which NH_2-terminus of TM4SF20 was recognized as a signal sequence in the absence of ceramide but not in the presence of the lipid. TRAM1 is an integral ER protein that was reported as an accessory factor in transmembrane protein biogenesis (Shao and Hegde, 2011; Voigt et al., 1996). Studies indicated that TRAM1 facilitates recognition of weak signal sequences that are less hydrophobic (Shao and Hegde, 2011), such as the signal sequence in TM4SF20. We hypothesized that TRAM1 may play an important role in recognizing signal sequence of TM4SF20. To test our hypothesis, we transfected A549/pTM4SF20 cells with two duplexes of siRNA targeting different regions of TRAM1. Such treatment knocked down expression of TRAM1 by more than 80% (Figure 18A). However, knockdown of TRAM1 had no effect on ceramide-induced alternative translocation of TM4SF20 (Figure 18B). We then transfected A549/pTM4SF20 cells with two duplexes of siRNA targeting different regions of TRAM2, the only other TRAM1 homologue expressed in A549 cells. This treatment knocked down expression of TRAM2 by 75% (Figure 18C). Knockdown of TRAM2 induced alternative translocation of TM4SF20 even in the absence of ceramide treatment (Figure 18D). These results suggested that TRAM2 but not TRAM1 was required to recognize NH_2-terminus of TM4SF20 as a signal sequence.

4.5 Discussion

The result shown above supported a new mechanism through which membrane proteins can adopt different topology through alternative usage of signal sequence. In the absence of ceramide, the NH_2-terminal sequence of TM4SF20 was recognized by TRAM2. This allowed NH_2-terminus of TM4SF20 to serve as a signal sequence that was cleaved by signal peptidase during translocation of the polypeptide across the ER. When cells were treated with ceramide, the NH_2-terminal sequence was no longer recognized as signal sequence, presumably because TRAM2 was inactivated by ceramide as the protein contained a domain predicted to bind the lipid. Consequently, the NH_2-terminus stays in the cytosol and adopts an opposite topology. This mechanism is termed as alternative translocation.

Because of alternative translocation, TM4SF20 proteins were modified differently. When signal sequence was recognized, the potential glycosylation sites between the third and fourth transmembrane stayed in the cytosol, preventing glycosylation on these sites. However, when TM4SF20 underwent alternative translocation upon ceramide treatment, the glycosylation sites were located in the ER lumen, resulting in N-linked glycosylation on these sites. Besides that, there were other post-translational modifications because PNGase F treatment did not completely shift the glycosylated band to the position of unglycosylated protein. It was likely that TM4SF20 were glycosylated by O-linked carbohydrates as well.

TRAM2 was found to be required for recognizing signal sequence of TM4SF20, but the underlying mechanism through which ceramide treatment blocked the function of TRAM2 remains unclear. TRAM2 is known to contain a TLC domain that is predicted to bind ceramide. Thus, ceramide binding may inactivate TRAM2 by inhibiting its interaction with either the NH_2-terminal sequence of TM4SF20 or Sec61.

TM4SF20 was identified as an inhibitory protein of RIP of CREB3L1. The fact that overexpressed TM4SF20 did not block ceramide-induced RIP of CREB3L1 suggested that alternative translocation of

TM4SF20 may alter the function of TM4SF20. In other words, the two differently orientated forms of TM4SF20 may play different roles in regulating RIP of CREB3L1. It is possible that the glycoslyated form of TM4SF20 is an inactive form that does not bind CREB3L1, allowing CREB3L1 going through RIP upon ceramide treatment. It is also possible that glycoslyated TM4SF20 not only fails to retain CREB3L1 in the ER but also preventing unglycosylated form of the protein from inhibiting cleavage of CREB3L1. Therefore two forms of TM4SF20 may have opposite roles in regulating RIP of CREB3L1. These possibilities need to be addressed in future study.

4.6 Chapter four figures

Figure 15. Ceramide induces glycosylation of TM4SF20.

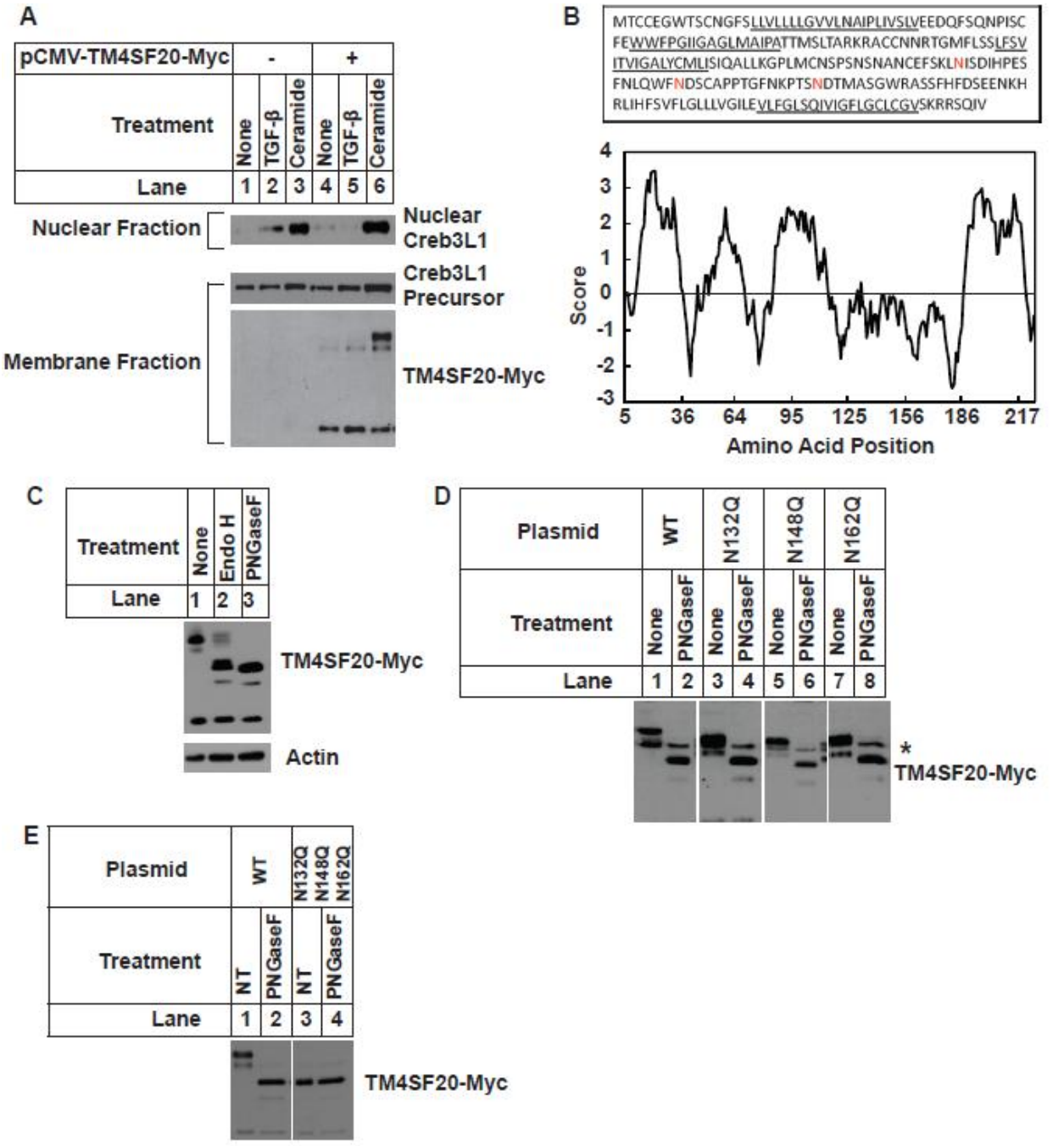

(A) On day 0, A549 cells were seeded at 4×10^5 cells per 60-mm dish. On day 1, cells were transfected with 1µg of pTK-HSV-CREB3L1 with or without 0.1µg of pCMV-TM4SF20-$(myc)_5$. The total amount of DNA was adjusted to 2µg/dish. After transfection, the cells were incubated for 16h with 1ng/ml TGF-β or 6µM C-6 ceramide. Cells were then harvested and separated into nuclear and membrane fractions, and

analyzed by immunoblot analysis with anti-HSV antibody to detect CREB3L1 and anti-myc antibody to detect TM4SF20.
(B) The amino acid sequence and hydropathy plot of TM4SF20. The putative membrane-spanning sequence was underlined. Potential *N*-linked glycosylation sites were highlighted in red. The residue-specific hydropathy index was calculated over a window of 9 residues by the method of Kyte and Doolittle (Kyte and Doolittle, 1982).
(C) On day 0, A549/pTM4SF20 cells were seeded at 4×10^5 cells per 60-mm dish. On day 1, after incubation with 6μM C-6 ceramide for 8hr, cells were harvested. Cell lysate were incubated in the absence and presence of the indicated glycosidase, subjected to SDS/PAGE and analyzed by immunoblot.
(D) On day 0, A549 cells were seeded at 4×10^5 cells per 60-mm dish. On day 1, cells were transfected with 2μg of pTK-TM4SF20-$(myc)_5$ or mutant plasmids. On day 2, cells were treated with 6μM C-6 ceramide for 8hr and harvested. Cell lysate were incubated in the absence and presence of PNGase F, subjected to SDS/PAGE and analyzed by immunoblot.
(E) Cells were set up as in (D) and transfected with 0.1μg of pCMV-TM4SF20-$(myc)_5$ or pCMV-TM4SF20(N132Q/N148Q/N163Q)-$(myc)_5$. Samples were prepared and analyzed as in (D)

Figure 16. Ceramide induces alternative translocation of TM4SF20.

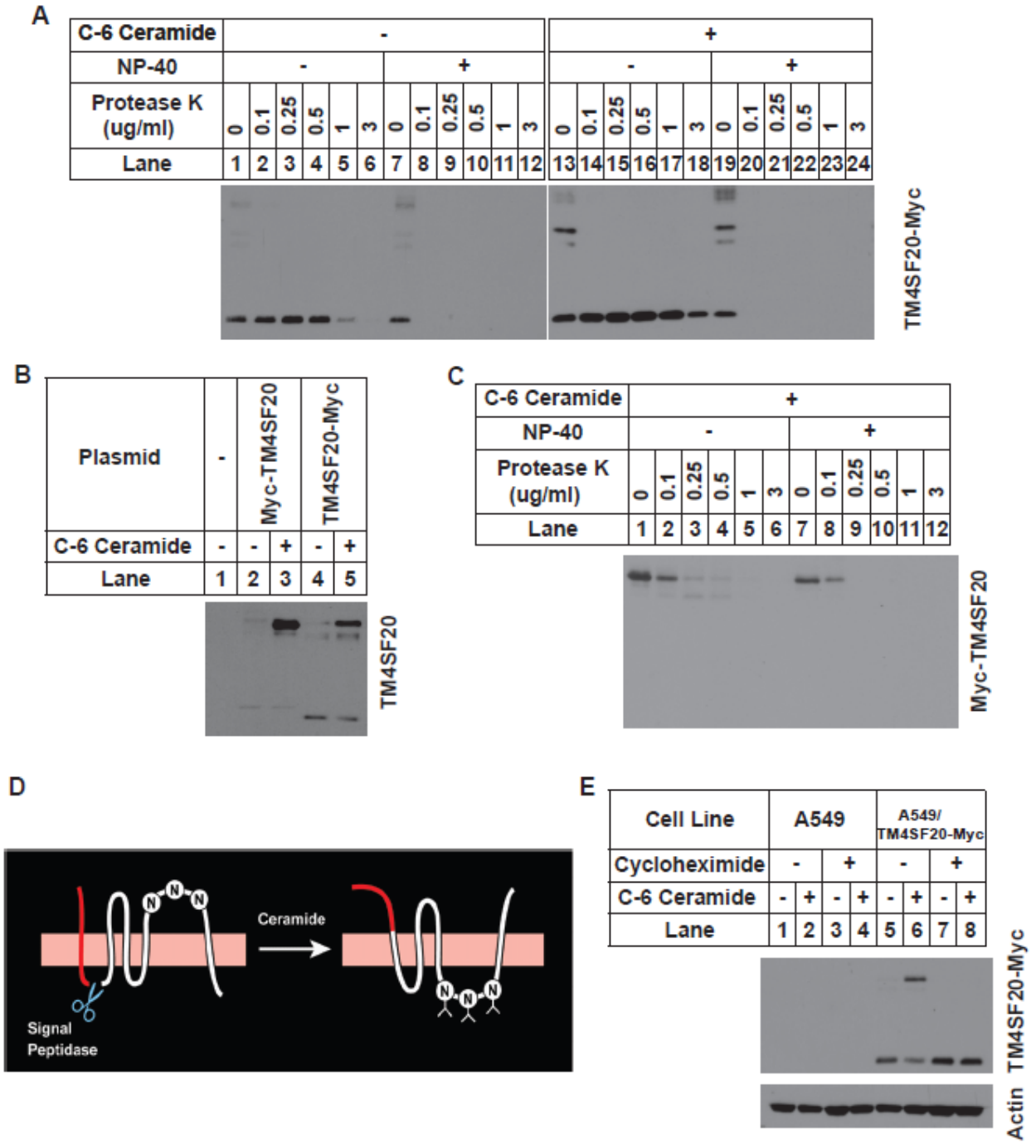

(A) On day 0, A549/TM4SF20 cells were seeded at 4×10^5 cells per 60-mm dish. On day 1, cells were left untreated or treated with 6μM C-6 ceramide for 8hr. Then cells were harvested for preparation of vesicle as described in Materials and Methods. Aliquots of the vesicles (50μg of protein) were treated with the indicated amount of protease K in a final volume of 50μl of bufferA2 in the absence or presence of 1% NP-40 as indicated. After incubation for 1h at 37˚C, the samples were then mixed with 5×laemmili buffer, boiled for 5min, and subjected to SDS/PAGE and immunoblot analysis with anti-myc antibody.

(B) On day 1, cells were transfected with 0.1μg of pCMV-TM4SF20-$(myc)_5$ or pCMV-$(myc)_5$-TM4SF20. The total amount of DNA was adjusted to 2μg/dish. On day 2, cells were left untreated or treated with 6μM C-6 ceramide for 8hr, harvested and analyzed by immunoblot.
(C) On day 0, A549 cells were seeded at 4×10^5 cells per 60-mm dish. On day 1, cells were transfected with 0.1μg of pCMV-$(myc)_5$–TM4SF20. The total amount of DNA was adjusted to 2μg/dish. On day 2, cells were treated with 6μM C-6 ceramide for 8hr, harvested and analyzed as described in Figure 16(A).
(D) In the absence of ceramide, NH_2-terminus of TM4SF20 is recognized as signal sequence and inserted into ER membrane and cleaved by singal peptidase. The loop between third and fourth membrane helix is located in the cytosol, preventing glycosylation. Upon ceramide treatment, the NH_2-terminus is no longer recognized as signal sequence and inserted into ER membrane. Consequently, TM4SF20 adopts an opposite topology and the loop between third and fourth membrane helix is facing ER lumen, resulting in *N*-linked glycosylation of three asparagines in the loop.
(E) On day 0, indicated cells were seeded at 4×10^5 cells per 60-mm dish. On day 1, cells were incubated in the absence or presence of cycloheximide or C-6 ceramide as indicated for 5hr. Then cells were harvested and analyzed by immunoblot analysis.

Figure 17. First transmembrane of TM4SF20 is important for alternative translocation

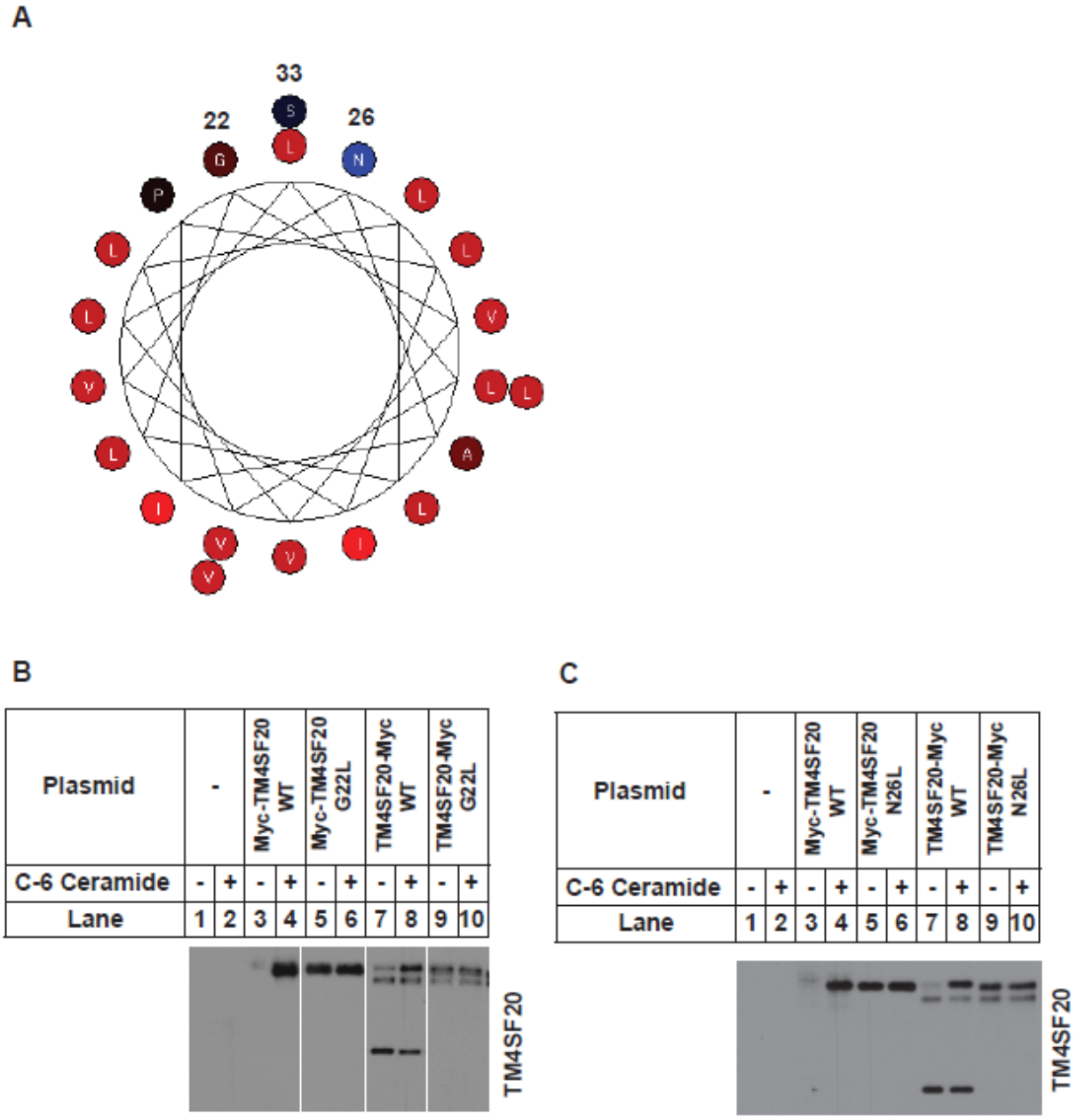

(A) Diagram of helical wheel analysis of first transmembrane domain of TM4SF20: G22 and N26 compose a less hydrophobic surface.
(B and C) On day 0, A549 cells were seeded at 4×10^5 cells per 60-mm dish. On day 1, cells were transfected with 0.1μg of indicated plasmid. The total amount of DNA was adjusted to 2μg/dish. On day 2, cells were treated with or without 6μM C-6 ceramide for 8hr and harvested. Cell lysates were subjected to SDS/PAGE and immunoblot analysis with anti-myc antibody.

Figure 18. TRAM2 is required for signal sequence recognition of TM4SF20.

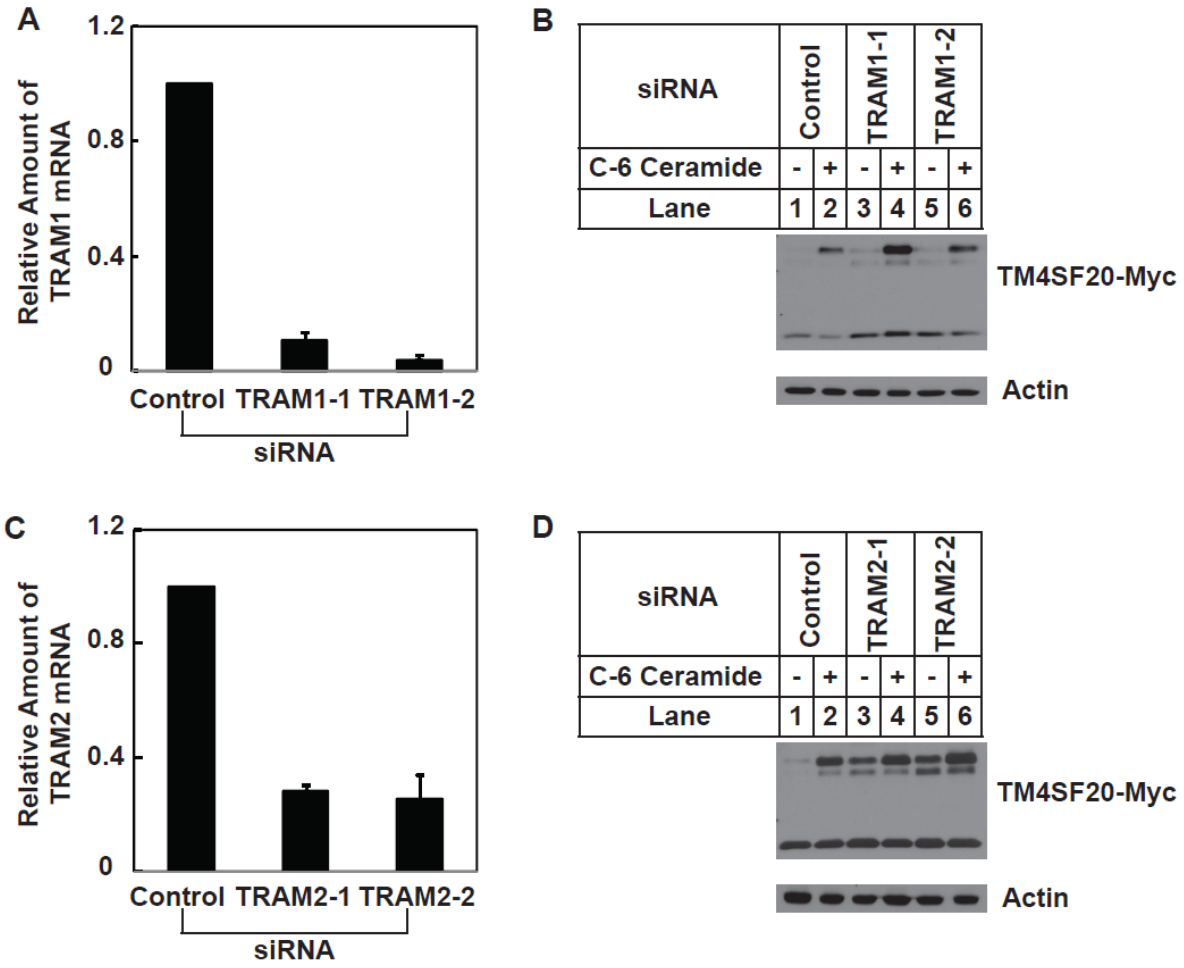

(A and B) On day 0, A549/TM4SF20-$(myc)_5$ cells were seeded at 1×10^5 cells per 60 mm dish. On day 1, the cells were transfected with indicted siRNAs. On day 3, cells were treated with or without 6μM C-6 ceramide. 8hr after the treatment, cells were harvested for quantification of TRAM1 mRNA by RT-QPCR (A), and immunoblot analysis (B).
(C and D) On day 0, A549/TM4SF20-$(myc)_5$ cells were seeded at 1×10^5 cells per 60 mm dish. On day 1, the cells were transfected with indicted siRNAs. On day 3, cells were treated with or without 6μM C-6 ceramide. 8hr after the treatment, cells were harvested for quantification of TRAM2 mRNA by RT-QPCR (C), and immunoblot analysis (D).

(A and C) Bar graphs are reported as mean ± S.E.M. of three independent experiments.

CHAPTER FIVE:

Conclusions and Future Directions

5.1 The role of CREB3L1 in fibrosis

Fibrosis is the pathological scarring process due to excessive accumulation of extracellular matrix especially collagen. Although the causes of fibrosis are very diverse and fibrosis of different organ is manifested by different features, there are similarities shared in all organs. One of the most prominent similarities is that TGF-β is overexpressed in all fibrotic tissue (Zeisberg and Kalluri, 2013) and plays an important role in inducing collagen expression. This made TGF-β pathway an attractive therapeutic target in all fibrotic organs. Actually, many drugs targeting the activity of TGF-β or anti-TGF-β neutralizing antibodies are investigated in preclinical studies or clinical trials (Akhurst and Hata, 2012). However, because of the multifunctional roles of TGF-β, systematic TGF-β inhibition could be potentially problematic. For example, TGF-β shows strong anti-proliferative (Akhurst and Derynck, 2001) and anti-inflammatory effects (Shull et al., 1992). Systematic inhibition of TGF-β activity might lead to severe side effects. Therefore, elucidating the mechanisms of the profibrotic action of TGF-β will provide more insights of targeting specific aspects of TGF-β pathway and minimize side effects. CREB3L1 is a transcription factor that is activated through regulated-intramembrane-proteolysis. Activation of CREB3L1 by TGF-β is required for long-term collagen production induced by TGF-β. More importantly, CREB3L1 is only required for activating genes required for the production of type I collagen but not other genes regulated by TGF-β. This may make CREB3L1 a better target in TGF-β pathway to treat fibrosis.

Animal studies are needed to study the *in vivo* function of CREB3L1 in fibrosis. We have dissected mice tissue and analyzed the expression of CREB3L1 in different organs. We found that CREB3L1 and TM4SF20 mRNA was highly expressed in colon. These results suggest that RIP of CREB3L1 may be responsible for colon fibrosis following colitis. This hypothesis may be tested by feeding mice with water containing sodium dextran sulfate, a treatment frequently induces colitis in mice. If our hypothesis is correct, such treatment is expected to induce cleavage of CREB3L1 by inhibiting expression of TM4SF20. If so, it will be interesting to determine whether mice deficient in CREB3L1 are more resistant to colon fibrosis following sodium dextran sulfate treatment.

5.2 Alternative translocation of TM4SF20

Alternative translocation is a process that membrane proteins are co-translationally translocated into the membrane in different orientation and result in different membrane topology of proteins. This is the first time this phenomenon was described. TM4SF20 is a membrane protein that has four transmembrane domains. It has two different topologies as shown in Figure 16D. In the absence of treatment, TM4SF20 exists as the unglycosylated form. Ceramide triggers alternative translocation of TM4SF20 and results in an opposite orientation of TM4SF20. The mechanism behind this alternative translocation is whether TRAM2 is able to recognize NH_2-terminus of TM4SF20 as a signal sequence. Despite this exciting discovery, many questions remain to be answered. These include 1) How TRAM2 recognizes signal sequence of TM4SF20? 2) How ceramide blocks this recognition and what is the binding site for ceramide of TRAM2? Since the TLC domain of TRAM2 is homologous to ceramide synthase, TLC domain could be the potential binding site of ceramide. 3) What is the function of these two different forms of TM4SF20? TM4SF20 was previously identified as an inhibitory protein of RIP of CREB3L1, but overexpressed TM4SF20 did not block ceramide-induced RIP of CREB3L1. Does the ceramide-induce form of TM4SF20 an inactive protein or it has the opposite function that can induce RIP of CREB3L1? 4) Are there any other proteins that also go through alternative translocation and what is the biological function of this process? TM4SF20 belongs to transmembrane 4 L six family that consists of twenty members, most of which remained uncharacterized. These proteins should be analyzed to determine if they also undergo alternative translocation in the presence of ceramide. The current study identifies TRAM2 as a protein required for alternative translocation of TM4SF20. In addition to TRAM2, mammalian cells also express TRAM1 and TRAM1L1, homologues of TRAM2 that also contain a TLC domain. Thus, proteins with NH_2-terminal sequences recognized by these two proteins may also undergo ceramide-induced alternative translocation. Identification of these proteins may not only broaden our understanding of alternative translocation, but also help us to understand the ceramide-mediated signaling

pathway. 5) Are there any other ways to induce alternative translocation? Signals affecting expression of TRAM proteins may also lead to alternative translocation of certain proteins.

APPENDIX

Table 1. mRNA increased in Huh-7 but not HRP4 cells in response to interferon treatment

Gene	NCBI nucleotide accession no.	Fold Increase in Huh-7 cells	Fold Increase in HRP4 cells
MX1	NM_002462	6.93	Absent
C1orf53	BI832220	6.34	1.75

Table 2. TGF-β-regulated genes

Gene Upregulated	NCBI nucleotide accession no.	Fold of Change
ADAM19	Y13786	18.14
LAMC2	NM_018891	17.83
CHRNA9	NM_017581	13.95
LCE3D	AB048288	13.61
ANGPTL4	AF169312	13.59
COL1A1	K01228	12.32
SERPINE1	NM_000602	9.75
MAF	AF055376	8.81
CTGF	M92934	8.36
RASGRP1	NM_005739	7.74
CLDN4	NM_001305	7.73
LBH	NM_030915	7.31
SPOCK1	AF231124	6.77
RHOU	AB051826	6.67
IL11	NM_000641	6.54
THBS1	NM_003246	6.01
TRIM9	AF220036	5.71
NAV2	NM_018162	5.65
FGF1	X59065	5.51
LRRC8C	AL136919	5.43
LMCD1	NM_014583	5.38
DAAM1	AK021890	5.25
TUFT1	NM_020127	5.05

Gene Downregulated	NCBI nucleotide accession no.	Fold of Change
SDPR	BF982174	7.16
TM4SF20	NM_024795	6.63

A549 cells treated with or without 1 ng/ml TGF-β for 12 h were harvested for microarray analysis. Genes whose expression was altered by TGF-β by more than 5 folds were listed with their NCBI nucleotide accession numbers. Genes encoding transmembrane proteins were highlighted in red. Among the highlighted genes, those encoding proteins that had not been confirmed to localize on plasma membranes were underlined.

BIBLIOGRAPH

Adams, C.M., Reitz, J., De Brabander, J.K., Feramisco, J.D., Li, L., Brown, M.S., and Goldstein, J.L. (2004). Cholesterol and 25-hydroxycholesterol inhibit activation of SREBPs by different mechanisms, both involving SCAP and Insigs. J Biol Chem *279*, 52772-52780.
Akhurst, R.J., and Derynck, R. (2001). TGF-beta signaling in cancer--a double-edged sword. Trends Cell Biol *11*, S44-51.
Akhurst, R.J., and Hata, A. (2012). Targeting the TGFbeta signalling pathway in disease. Nat Rev Drug Discov *11*, 790-811.
Araya, J., and Nishimura, S.L. (2010). Fibrogenic reactions in lung disease. Annu Rev Pathol *5*, 77-98.
Bi, W.R., Yang, C.Q., and Shi, Q. (2012). Transforming growth factor-beta1 induced epithelial-mesenchymal transition in hepatic fibrosis. Hepatogastroenterology *59*, 1960-1963.
Binder, M., Kochs, G., Bartenschlager, R., and Lohmann, V. (2007). Hepatitis C virus escape from the interferon regulatory factor 3 pathway by a passive and active evasion strategy. Hepatology *46*, 1365-1374.
Blight, K.J., McKeating, J.A., and Rice, C.M. (2002). Highly permissive cell lines for subgenomic and genomic hepatitis C virus RNA replication. J Virol *76*, 13001-13014.
Brown, M.S., and Goldstein, J.L. (2009). Cholesterol feedback: from Schoenheimer's bottle to Scap's MELADL. J Lipid Res *50 Suppl*, S15-27.
Brown, M.S., Ye, J., Rawson, R.B., and Goldstein, J.L. (2000). Regulated intramembrane proteolysis: a control mechanism conserved from bacteria to humans. Cell *100*, 391-398.
Burch, M.L., Zheng, W., and Little, P.J. (2011). Smad linker region phosphorylation in the regulation of extracellular matrix synthesis. Cell Mol Life Sci *68*, 97-107.
Cai, Z., Zhang, C., Chang, K.S., Jiang, J., Ahn, B.C., Wakita, T., Liang, T.J., and Luo, G. (2005). Robust production of infectious hepatitis C virus (HCV) from stably HCV cDNA-transfected human hepatoma cells. J Virol *79*, 13963-13973.
Calmon, M.F., Rodrigues, R.V., Kaneto, C.M., Moura, R.P., Silva, S.D., Mota, L.D., Pinheiro, D.G., Torres, C., de Carvalho, A.F., Cury, P.M., *et al.* (2009). Epigenetic silencing of CRABP2 and MX1 in head and neck tumors. Neoplasia *11*, 1329-1339.
Chapman, H.A. (2011). Epithelial-mesenchymal interactions in pulmonary fibrosis. Annu Rev Physiol *73*, 413-435.
Chen, S.L., and Morgan, T.R. (2006). The natural history of hepatitis C virus (HCV) infection. Int J Med Sci *3*, 47-52.
Cheng, J.C., and Leung, P.C. (2011). Type I collagen down-regulates E-cadherin expression by increasing PI3KCA in cancer cells. Cancer Lett *304*, 107-116.
Christman, J.K. (2002). 5-Azacytidine and 5-aza-2'-deoxycytidine as inhibitors of DNA methylation: mechanistic studies and their implications for cancer therapy. Oncogene *21*, 5483-5495.
Deaton, A.M., and Bird, A. (2011). CpG islands and the regulation of transcription. Genes Dev *25*, 1010-1022.

DeBose-Boyd, R.A., Brown, M.S., Li, W.P., Nohturfft, A., Goldstein, J.L., and Espenshade, P.J. (1999). Transport-dependent proteolysis of SREBP: relocation of site-1 protease from Golgi to ER obviates the need for SREBP transport to Golgi. Cell *99*, 703-712.
Denard, B., Lee, C., and Ye, J. (2012). Doxorubicin blocks proliferation of cancer cells through proteolytic activation of CREB3L1. Elife *1*, e00090.
Denard, B., Seemann, J., Chen, Q., Gay, A., Huang, H., Chen, Y., and Ye, J. (2011). The membrane-bound transcription factor CREB3L1 is activated in response to virus infection to inhibit proliferation of virus-infected cells. Cell Host Microbe *10*, 65-74.
Derynck, R., and Zhang, Y.E. (2003). Smad-dependent and Smad-independent pathways in TGF-beta family signalling. Nature *425*, 577-584.
Desmond, J.C., Raynaud, S., Tung, E., Hofmann, W.K., Haferlach, T., and Koeffler, H.P. (2007). Discovery of epigenetically silenced genes in acute myeloid leukemias. Leukemia *21*, 1026-1034.
Dooley, S., and ten Dijke, P. (2012). TGF-beta in progression of liver disease. Cell Tissue Res *347*, 245-256.
Doyle, J.J., Gerber, E.E., and Dietz, H.C. (2012). Matrix-dependent perturbation of TGFbeta signaling and disease. FEBS Lett *586*, 2003-2015.
Edgley, A.J., Krum, H., and Kelly, D.J. (2012). Targeting fibrosis for the treatment of heart failure: a role for transforming growth factor-beta. Cardiovasc Ther *30*, e30-40.
Feng, X.H., and Derynck, R. (2005). Specificity and versatility in tgf-beta signaling through Smads. Annu Rev Cell Dev Biol *21*, 659-693.
Fensterl, V., and Sen, G.C. (2011). The ISG56/IFIT1 gene family. J Interferon Cytokine Res *31*, 71-78.
Feramisco, J.D., Goldstein, J.L., and Brown, M.S. (2004). Membrane topology of human insig-1, a protein regulator of lipid synthesis. J Biol Chem *279*, 8487-8496.
Frese, M., Pietschmann, T., Moradpour, D., Haller, O., and Bartenschlager, R. (2001). Interferon-alpha inhibits hepatitis C virus subgenomic RNA replication by an MxA-independent pathway. J Gen Virol *82*, 723-733.
Gong, Y., Lee, J.N., Lee, P.C., Goldstein, J.L., Brown, M.S., and Ye, J. (2006). Sterol-regulated ubiquitination and degradation of Insig-1 creates a convergent mechanism for feedback control of cholesterol synthesis and uptake. Cell Metab *3*, 15-24.
Gordon, K.J., and Blobe, G.C. (2008). Role of transforming growth factor-beta superfamily signaling pathways in human disease. Biochim Biophys Acta *1782*, 197-228.
Habashi, J.P., Doyle, J.J., Holm, T.M., Aziz, H., Schoenhoff, F., Bedja, D., Chen, Y., Modiri, A.N., Judge, D.P., and Dietz, H.C. (2011). Angiotensin II type 2 receptor signaling attenuates aortic aneurysm in mice through ERK antagonism. Science *332*, 361-365.
Haller, O., Staeheli, P., and Kochs, G. (2007). Interferon-induced Mx proteins in antiviral host defense. Biochimie *89*, 812-818.
Hannun, Y.A., and Obeid, L.M. (2008). Principles of bioactive lipid signalling: lessons from sphingolipids. Nat Rev Mol Cell Biol *9*, 139-150.
Hawkins, J.L., Robbins, M.D., Warren, L.C., Xia, D., Petras, S.F., Valentine, J.J., Varghese, A.H., Wang, I.K., Subashi, T.A., Shelly, L.D., *et al.* (2008). Pharmacologic inhibition of site 1 protease activity inhibits sterol regulatory element-binding protein processing and reduces lipogenic enzyme gene expression and lipid synthesis in cultured cells and experimental animals. J Pharmacol Exp Ther *326*, 801-808.

Holm, T.M., Habashi, J.P., Doyle, J.J., Bedja, D., Chen, Y., van Erp, C., Lindsay, M.E., Kim, D., Schoenhoff, F., Cohn, R.D., *et al.* (2011). Noncanonical TGFbeta signaling contributes to aortic aneurysm progression in Marfan syndrome mice. Science *332*, 358-361.
Horton, J.D., Shah, N.A., Warrington, J.A., Anderson, N.N., Park, S.W., Brown, M.S., and Goldstein, J.L. (2003). Combined analysis of oligonucleotide microarray data from transgenic and knockout mice identifies direct SREBP target genes. Proc Natl Acad Sci U S A *100*, 12027-12032.
Huang, H., Sun, F., Owen, D.M., Li, W., Chen, Y., Gale, M., Jr., and Ye, J. (2007). Hepatitis C virus production by human hepatocytes dependent on assembly and secretion of very low-density lipoproteins. Proc Natl Acad Sci U S A *104*, 5848-5853.
Iverson, C., Larson, G., Lai, C., Yeh, L.T., Dadson, C., Weingarten, P., Appleby, T., Vo, T., Maderna, A., Vernier, J.M., *et al.* (2009). RDEA119/BAY 869766: a potent, selective, allosteric inhibitor of MEK1/2 for the treatment of cancer. Cancer Res *69*, 6839-6847.
Kang, T., Zhao, Y.G., Pei, D., Sucic, J.F., and Sang, Q.X. (2002). Intracellular activation of human adamalysin 19/disintegrin and metalloproteinase 19 by furin occurs via one of the two consecutive recognition sites. J Biol Chem *277*, 25583-25591.
Kasai, H., Allen, J.T., Mason, R.M., Kamimura, T., and Zhang, Z. (2005). TGF-beta1 induces human alveolar epithelial to mesenchymal cell transition (EMT). Respir Res *6*, 56.
Katze, M.G., He, Y., and Gale, M., Jr. (2002). Viruses and interferon: a fight for supremacy. Nat Rev Immunol *2*, 675-687.
Kisseleva, T., and Brenner, D.A. (2008). Mechanisms of fibrogenesis. Exp Biol Med (Maywood) *233*, 109-122.
Kyte, J., and Doolittle, R.F. (1982). A simple method for displaying the hydropathic character of a protein. J Mol Biol *157*, 105-132.
Lan, H.Y. (2011). Diverse roles of TGF-beta/Smads in renal fibrosis and inflammation. Int J Biol Sci *7*, 1056-1067.
Lauer, G.M., and Walker, B.D. (2001). Hepatitis C virus infection. N Engl J Med *345*, 41-52.
Lee, J.N., Song, B., DeBose-Boyd, R.A., and Ye, J. (2006). Sterol-regulated degradation of Insig-1 mediated by the membrane-bound ubiquitin ligase gp78. J Biol Chem *281*, 39308-39315.
Lee, J.N., Zhang, X., Feramisco, J.D., Gong, Y., and Ye, J. (2008). Unsaturated fatty acids inhibit proteasomal degradation of Insig-1 at a postubiquitination step. J Biol Chem *283*, 33772-33783.
Li, A., Zhou, T., Guo, L., and Si, J. (2010). Collagen type I regulates beta-catenin tyrosine phosphorylation and nuclear translocation to promote migration and proliferation of gastric carcinoma cells. Oncol Rep *23*, 1247-1255.
Liang, G., Yang, J., Horton, J.D., Hammer, R.E., Goldstein, J.L., and Brown, M.S. (2002). Diminished hepatic response to fasting/refeeding and liver X receptor agonists in mice with selective deficiency of sterol regulatory element-binding protein-1c. J Biol Chem *277*, 9520-9528.
Lindenbach, B.D., and Rice, C.M. (2005). Unravelling hepatitis C virus replication from genome to function. Nature *436*, 933-938.
Lohmann, V., Korner, F., Koch, J., Herian, U., Theilmann, L., and Bartenschlager, R. (1999). Replication of subgenomic hepatitis C virus RNAs in a hepatoma cell line. Science *285*, 110-113.
Martinek, N., Shahab, J., Sodek, J., and Ringuette, M. (2007). Is SPARC an evolutionarily conserved collagen chaperone? J Dent Res *86*, 296-305.

Massague, J. (2008). TGFbeta in Cancer. Cell *134*, 215-230.
Massague, J. (2012). TGFbeta signalling in context. Nat Rev Mol Cell Biol *13*, 616-630.
Morad, S.A., and Cabot, M.C. (2013). Ceramide-orchestrated signalling in cancer cells. Nat Rev Cancer *13*, 51-65.
Moradpour, D., Penin, F., and Rice, C.M. (2007). Replication of hepatitis C virus. Nat Rev Microbiol *5*, 453-463.
Mu, Y., Gudey, S.K., and Landstrom, M. (2012). Non-Smad signaling pathways. Cell Tissue Res *347*, 11-20.
Murakami, T., Kondo, S., Ogata, M., Kanemoto, S., Saito, A., Wanaka, A., and Imaizumi, K. (2006). Cleavage of the membrane-bound transcription factor OASIS in response to endoplasmic reticulum stress. J Neurochem *96*, 1090-1100.
Murakami, T., Saito, A., Hino, S., Kondo, S., Kanemoto, S., Chihara, K., Sekiya, H., Tsumagari, K., Ochiai, K., Yoshinaga, K., *et al.* (2009). Signalling mediated by the endoplasmic reticulum stress transducer OASIS is involved in bone formation. Nat Cell Biol *11*, 1205-1211.
Naka, K., Abe, K., Takemoto, K., Dansako, H., Ikeda, M., Shimotohno, K., and Kato, N. (2006). Epigenetic silencing of interferon-inducible genes is implicated in interferon resistance of hepatitis C virus replicon-harboring cells. J Hepatol *44*, 869-878.
Nguyen, V.T., Ndoye, A., and Grando, S.A. (2000). Novel human alpha9 acetylcholine receptor regulating keratinocyte adhesion is targeted by Pemphigus vulgaris autoimmunity. Am J Pathol *157*, 1377-1391.
Nieto, M.A. (2011). The ins and outs of the epithelial to mesenchymal transition in health and disease. Annu Rev Cell Dev Biol *27*, 347-376.
Nohturfft, A., Yabe, D., Goldstein, J.L., Brown, M.S., and Espenshade, P.J. (2000). Regulated step in cholesterol feedback localized to budding of SCAP from ER membranes. Cell *102*, 315-323.
Olmstead, A.D., Knecht, W., Lazarov, I., Dixit, S.B., and Jean, F. (2012). Human subtilase SKI-1/S1P is a master regulator of the HCV Lifecycle and a potential host cell target for developing indirect-acting antiviral agents. PLoS Pathog *8*, e1002468.
Omori, Y., Imai, J., Suzuki, Y., Watanabe, S., Tanigami, A., and Sugano, S. (2002). OASIS is a transcriptional activator of CREB/ATF family with a transmembrane domain. Biochem Biophys Res Commun *293*, 470-477.
Pietschmann, T., Lohmann, V., Rutter, G., Kurpanek, K., and Bartenschlager, R. (2001). Characterization of cell lines carrying self-replicating hepatitis C virus RNAs. J Virol *75*, 1252-1264.
Radhakrishnan, A., Sun, L.P., Kwon, H.J., Brown, M.S., and Goldstein, J.L. (2004). Direct binding of cholesterol to the purified membrane region of SCAP: mechanism for a sterol-sensing domain. Mol Cell *15*, 259-268.
Rentz, T.J., Poobalarahi, F., Bornstein, P., Sage, E.H., and Bradshaw, A.D. (2007). SPARC regulates processing of procollagen I and collagen fibrillogenesis in dermal fibroblasts. J Biol Chem *282*, 22062-22071.
Rosenbloom, J., Castro, S.V., and Jimenez, S.A. (2010). Narrative review: fibrotic diseases: cellular and molecular mechanisms and novel therapies. Ann Intern Med *152*, 159-166.
Sadler, A.J., and Williams, B.R. (2008). Interferon-inducible antiviral effectors. Nat Rev Immunol *8*, 559-568.

Sakai, J., Duncan, E.A., Rawson, R.B., Hua, X., Brown, M.S., and Goldstein, J.L. (1996). Sterol-regulated release of SREBP-2 from cell membranes requires two sequential cleavages, one within a transmembrane segment. Cell *85*, 1037-1046.
Sakai, J., Nohturfft, A., Cheng, D., Ho, Y.K., Brown, M.S., and Goldstein, J.L. (1997). Identification of complexes between the COOH-terminal domains of sterol regulatory element-binding proteins (SREBPs) and SREBP cleavage-activating protein. J Biol Chem *272*, 20213-20221.
Sakai, J., Rawson, R.B., Espenshade, P.J., Cheng, D., Seegmiller, A.C., Goldstein, J.L., and Brown, M.S. (1998). Molecular identification of the sterol-regulated luminal protease that cleaves SREBPs and controls lipid composition of animal cells. Mol Cell *2*, 505-514.
Scholle, F., Li, K., Bodola, F., Ikeda, M., Luxon, B.A., and Lemon, S.M. (2004). Virus-host cell interactions during hepatitis C virus RNA replication: impact of polyprotein expression on the cellular transcriptome and cell cycle association with viral RNA synthesis. J Virol *78*, 1513-1524.
Sever, N., Lee, P.C., Song, B.L., Rawson, R.B., and Debose-Boyd, R.A. (2004). Isolation of mutant cells lacking Insig-1 through selection with SR-12813, an agent that stimulates degradation of 3-hydroxy-3-methylglutaryl-coenzyme A reductase. J Biol Chem *279*, 43136-43147.
Shao, S., and Hegde, R.S. (2011). Membrane protein insertion at the endoplasmic reticulum. Annu Rev Cell Dev Biol *27*, 25-56.
Shen, J., Chen, X., Hendershot, L., and Prywes, R. (2002). ER stress regulation of ATF6 localization by dissociation of BiP/GRP78 binding and unmasking of Golgi localization signals. Dev Cell *3*, 99-111.
Shintani, Y., Fukumoto, Y., Chaika, N., Svoboda, R., Wheelock, M.J., and Johnson, K.R. (2008a). Collagen I-mediated up-regulation of N-cadherin requires cooperative signals from integrins and discoidin domain receptor 1. J Cell Biol *180*, 1277-1289.
Shintani, Y., Maeda, M., Chaika, N., Johnson, K.R., and Wheelock, M.J. (2008b). Collagen I promotes epithelial-to-mesenchymal transition in lung cancer cells via transforming growth factor-beta signaling. Am J Respir Cell Mol Biol *38*, 95-104.
Shull, M.M., Ormsby, I., Kier, A.B., Pawlowski, S., Diebold, R.J., Yin, M., Allen, R., Sidman, C., Proetzel, G., Calvin, D., *et al.* (1992). Targeted disruption of the mouse transforming growth factor-beta 1 gene results in multifocal inflammatory disease. Nature *359*, 693-699.
Sumpter, R., Jr., Loo, Y.M., Foy, E., Li, K., Yoneyama, M., Fujita, T., Lemon, S.M., and Gale, M., Jr. (2005). Regulating intracellular antiviral defense and permissiveness to hepatitis C virus RNA replication through a cellular RNA helicase, RIG-I. J Virol *79*, 2689-2699.
Sumpter, R., Jr., Wang, C., Foy, E., Loo, Y.M., and Gale, M., Jr. (2004). Viral evolution and interferon resistance of hepatitis C virus RNA replication in a cell culture model. J Virol *78*, 11591-11604.
Tsukita, S., and Furuse, M. (2002). Claudin-based barrier in simple and stratified cellular sheets. Curr Opin Cell Biol *14*, 531-536.
Verrecchia, F., and Mauviel, A. (2007). Transforming growth factor-beta and fibrosis. World J Gastroenterol *13*, 3056-3062.
Voigt, S., Jungnickel, B., Hartmann, E., and Rapoport, T.A. (1996). Signal sequence-dependent function of the TRAM protein during early phases of protein transport across the endoplasmic reticulum membrane. J Cell Biol *134*, 25-35.

Walter, P., and Ron, D. (2011). The unfolded protein response: from stress pathway to homeostatic regulation. Science *334*, 1081-1086.
Wang, C., Gale, M., Jr., Keller, B.C., Huang, H., Brown, M.S., Goldstein, J.L., and Ye, J. (2005). Identification of FBL2 as a geranylgeranylated cellular protein required for hepatitis C virus RNA replication. Mol Cell *18*, 425-434.
Weber, M., Davies, J.J., Wittig, D., Oakeley, E.J., Haase, M., Lam, W.L., and Schubeler, D. (2005). Chromosome-wide and promoter-specific analyses identify sites of differential DNA methylation in normal and transformed human cells. Nat Genet *37*, 853-862.
Winter, E., and Ponting, C.P. (2002). TRAM, LAG1 and CLN8: members of a novel family of lipid-sensing domains? Trends Biochem Sci *27*, 381-383.
Wright, M.D., Ni, J., and Rudy, G.B. (2000). The L6 membrane proteins--a new four-transmembrane superfamily. Protein Sci *9*, 1594-1600.
Yabe, D., Brown, M.S., and Goldstein, J.L. (2002). Insig-2, a second endoplasmic reticulum protein that binds SCAP and blocks export of sterol regulatory element-binding proteins. Proc Natl Acad Sci U S A *99*, 12753-12758.
Yang, T., Espenshade, P.J., Wright, M.E., Yabe, D., Gong, Y., Aebersold, R., Goldstein, J.L., and Brown, M.S. (2002). Crucial step in cholesterol homeostasis: sterols promote binding of SCAP to INSIG-1, a membrane protein that facilitates retention of SREBPs in ER. Cell *110*, 489-500.
Ye, J., and DeBose-Boyd, R.A. (2011). Regulation of cholesterol and fatty acid synthesis. Cold Spring Harb Perspect Biol *3*.
Ye, J., Rawson, R.B., Komuro, R., Chen, X., Dave, U.P., Prywes, R., Brown, M.S., and Goldstein, J.L. (2000). ER stress induces cleavage of membrane-bound ATF6 by the same proteases that process SREBPs. Mol Cell *6*, 1355-1364.
Zavadil, J., and Bottinger, E.P. (2005). TGF-beta and epithelial-to-mesenchymal transitions. Oncogene *24*, 5764-5774.
Zeisberg, M., and Kalluri, R. (2013). Cellular mechanisms of tissue fibrosis. 1. Common and organ-specific mechanisms associated with tissue fibrosis. Am J Physiol Cell Physiol *304*, C216-225.